ChemComm

ROYAL SOCIETY OF CHEMISTRY

FEATURE ARTICLE

View Article Online
View Journal | View Issue

Cite this: *Chem. Commun.*, 2023, **59**, 3206

Strategies to quench quantum tunneling of magnetization in lanthanide single molecule magnets

Abinash Swain, Tanu Sharma and Gopalan Rajaraman *

Received 8th November 2022,
Accepted 7th February 2023

DOI: 10.1039/d2cc06041h

rsc.li/chemcomm

Enhancing blocking temperature (T_B) is one of the holy grails in Single Molecule Magnets(SMMs), as any future potential application in this class of molecules is directly correlated to this parameter. Among many factors contributing to a reduction of T_B value, Quantum Tunnelling of Magnetisation (QTM), a phenomenon that is a curse or a blessing based on the application sought after, tops the list. Theoretical tools based on density functional and *ab initio* CASSCF/RASSI-SO methods have played a prominent role in estimating various spin Hamiltonian parameters and establishing the mechanism of magnetization relaxation in this class of molecules. Particularly, various strategies to quench QTM effects go hand-in-hand with experiments, and different methods proposed to quell QTM effects are scattered in the literature. In this perspective, we have explored various approaches that are proposed in the literature to quench QTM effects, and these include the role of (i) local symmetry of lanthanides, (ii) super-exchange interaction in {3d–4f} complexes, (iii) direct-exchange interaction in {radical-4f} and metal–metal bonded complexes to suppress the QTM, (iv) utilizing external stimuli such as an electric field or pressure to modulate the QTM and (v) avoiding QTM effects by stabilising toroidal states in 4f and {3d–4f} clusters. We believe the strategies summarized here will help to design new-generation SMMs.

1. Introduction

The Single-Molecule Magnets (SMMs)[1] are the impending candidate for next-generation information storage and quantum computing in devices.[2–5] These are the class of molecules for which magnetic bistability can be achieved at the molecular level

Department of Chemistry, IIT Bombay, Powai, Mumbai – 400076, India.
E-mail: rajaraman@chem.iitb.ac.in

Abinash Swain

Abinash Swain was born in Bargarh (Odisha), India and received a BSc in Chemistry from BJB College, Utkal University, Bhubaneswar, in 2013. He obtained his MSc from the School of Chemistry, University of Hyderabad, in 2015 and received UGC-JRF scholarships to complete his PhD under the supervision of Prof. Gopalan Rajaraman at IIT Bombay, India, in 2022. His research interests focus on modelling molecular nanomagnets, with special emphasis on the modelling and synthesis of Single-Molecule Toroics and analysing the ferrotoroidic behaviour of lanthanide metal complexes using DFT and ab initio calculations.

Tanu Sharma

Tanu Sharma, born in Pathankot (Punjab), India, graduated in 2017 with a BSc (Hons School) and an MSc (Hons School) in chemistry from Guru Nanak Dev University in Amritsar, India and received CSIR-JRF scholarships to undertake her PhD under the supervision of Prof. Gopalan Rajaraman at IIT Bombay, India. Her research focuses on modelling molecular nanomagnets, focusing on lanthanide-based SMMs employing ab initio and DFT approaches. Further, she is exploring various endohedral metallofullerene as SMM employing these tools to predict new generation SMMs.

so that magnetic hysteresis can be observed below blocking temperature (T_B).[6,7] The disadvantages of the current generation bulk nano-magnetic materials can be omitted by SMMs as these state of art complexes can now mimic the super-paramagnetism at the molecular level.[8] However, the practical application of these molecules is still limited. There is more than one way to ascertain the performance of SMMs. The most acceptable and practical way would be blocking temperature (T_B), a temperature below which the magnetization is frozen.[9] Over the years, the blocking temperature definition has been diversified, and at least three common protocols are employed to measure the blocking temperature, which we would like to term T_B^{FZ}, T_B^{hys}, and T_B^{100} so that cross-comparison among different molecules is straightforward.[9] The T_B^{FZ} can be defined as the temperature at which the field-cooled (FC) and zero-field-cooled (FC) modes of the magnetic susceptibility *vs.* temperature plots overlap with each other, whereas T_B^{hys} can be defined as the temperature at which the coercivity of hysteresis loop collapses.[9] According to Sessoli and Gatteschi *et al.*, T_B^{100} is the temperature at which magnetization takes one hundred seconds to relax.[9] The other parameters by which the SMM properties can be ascertained are the barrier for the magnetic reversal (U_{eff}), which is defined as the energy needed to flip the orientation of the magnetic states, and magnetic relaxation times (τ), which is defined as the time taken for the magnetization to relax. Because of the limiting value of blocking temperature of <80 K achieved so far,[10] the use of these molecules in the industry is still a challenge. Attaining room temperature T_B values is one of the foremost challenges in the field of molecular magnetism, and the second one would be to retain them on the surface for any potential applications proposed.[11–13]

In the initial years since the discovery of $[Mn_{12}O_{12}(OAc)_{16}(H_2O)_4]$[14] as the first SMMs, the focus pertained to attaining a large spin ground state (S) and a large axial zero-field splitting parameter (D), which were correlated to the U_{eff} value by the following eqn (1) for integer spin system,[15]

$$U_{eff} = DS^2 \quad (1)$$

However, later it was realized that despite having very large ground spin states, several polynuclear metal clusters (such as Mn_{84}, Mn_{19}, Mo_6Mn_9, Fe_{19}, and Mn_{25} cages, to name a few),[16–20] the barriers for magnetic reversal were very small, and several works highlighted the inverse relationship between the spin of the ground state and D values.[21] As the magnetic anisotropy is very challenging to tune in transition metal clusters, the focus was shifted to other systems possessing moderate S values but large D values, such as mononuclear transition metal complexes. While there has been some success in this endeavour in recent years, the S value is not substantial to yield larger barrier heights.[22–24] In the meantime, an alternative class of molecules, based on lanthanide emerged with the discovery of $[TbPc_2]$ complex[25] by Ishikawa, and the paradigm shifted towards the Lanthanides as they have very large anisotropy (except Ln with ground electronic terms $^1S_0$ and $^8S_{7/2}$) due to large spin–orbit coupling offered by the unquenched orbital momentum[26,27](Fig. 1).

As the crystal field splitting can be modulated by varying the ligand field around the lanthanides, this quickly picked up the pace, with chemists reporting several new SMMs based on lanthanides, with Dy^{III} being the most successful, a design criterion was surely lacking. Rinehart and Long reported this based on simple ligand field theory, where lanthanides are classified as prolate and oblate based on their ground state m_J electron density and proposed various synthetic strategies to obtain lanthanide SMMs.[27] This was hugely popular among chemists and has yielded numerous performant SMMs based on lanthanide in a short span of time.[28–32] Among lanthanides, if the correct crystal field is chosen, Tb^{III}, Dy^{III}, Ho^{III}, and Er^{III} can yield large m_J ground states.[9] Among these ions, Dy^{III} and Er^{III} are Kramers ions, offering bistability if an appropriate ligand field is applied. It has been reported earlier that the axial ligand field favours oblate charge distribution, whereas strong equatorial ligands favour prolate charge distribution. Thus highest m_J ground state is stabilised for different geometries of the ligand field for different ions (axial for Pr^{III}, Tb^{III}, Dy^{III}, Nd^{III}, and Ho^{III}, so-called oblate ions; equatorial for Pm^{III}, Tm^{III}, Yb^{III}, and Er^{III}, so-called prolate ions).[27,33] The representations of the ground state (with the largest m_J) shape for all the Lanthanides has been provided in Fig. 2, indicating the oblate and prolate nature of the ground state m_J levels. The symmetry around the Ln^{III} centre, as well as the approach of the ligand field (whether axial or equatorial), is needed depending upon the nature of the ions, which is strongly correlated to the U_{eff} barrier.[28,34] While this offers a way to design SMMs to stabilize a large m_J as the ground state, the relaxation often happens *via* excited states, which have different electron densities. Further, the gap between the m_J levels, which is a crucial parameter for the performance of SMMs, is hard to predict unless a quantitative approach is employed and full relaxation mechanisms are established.

1.1. Magnetic relaxation pathways

The magnetic properties originate from the molecular level has quantum characteristics. Hence the magnetic relaxation

Gopalan Rajaraman

Gopalan Rajaraman (born in Thanjavur, India) received his PhD at the University of Manchester, UK, in 2004. He then undertook postdoctoral stays at the University of Heidelberg, Germany (2005–2007) and the University of Florence, Italy (2007–2009). In December 2009, he joined IIT Bombay, India as an assistant professor and became a professor in 2018. His research employs electronic structure methods to understand the structure, properties and reactivity of molecules possessing unpaired electrons (open-shell systems). In addition to modelling molecular magnets, his group actively pursued research in modelling bio-mimic reactions catalysed by high-valent metal-oxo/imido complexes.

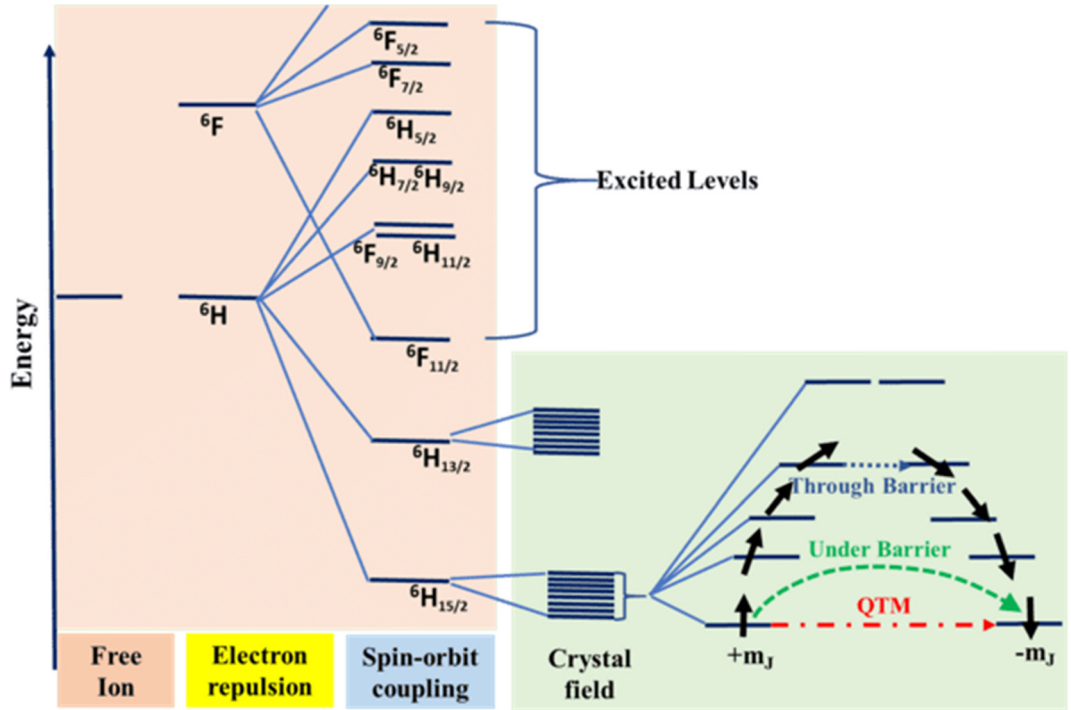

Fig. 1 The energy level splitting for a $4f^9$ (Dy^{III}) ion placed in an axial electrostatic crystal field, as well as the possible relaxation pathways. Higher-energy spin states are abbreviated for clarity. Reproduced from ref. 34 with permission from [Royal Society of Chemistry], copyright [2022].

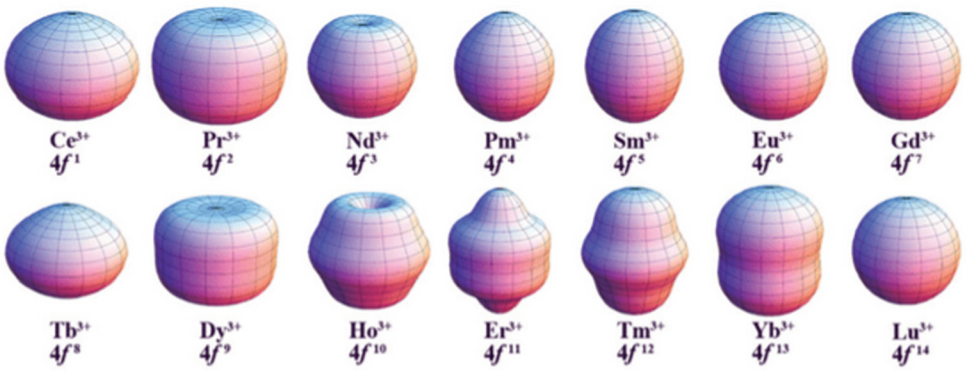

Fig. 2 The shape of different lanthanide ions in their highest m_J states. Reproduced from ref. 33 with permission from [Royal Society of Chemistry], copyright [2015].

processes are widely diverse, complicated, and very much subjected to various external factors such as magnetic and electric fields, temperatures, pressure, and internal factors such as hyperfine interactions and inter/intramolecular interactions.[22,35] Among all processes, the most common magnetic relaxation mechanisms are the Orbach and Raman, which occur due to spin–phonon coupling, and Quantum tunnelling of magnetisation (QTM), which is a temperature-independent phenomenon. A thermally assisted QTM process among excited m_J levels is also possible through which the relaxation occurs. Orbach and Raman are the two phonon relaxation processes, while direct methods involve a single phonon only.[8] In an ideal stepwise Orbach process, the system absorbs a phonon from the surrounding having precisely the same energy between the ground and the specific low-lying excited states ($\hbar\omega_1/2\pi$), causing the excitation to the excited state. This will relax to the ground state by emitting new phonons ($\hbar\omega_2/2\pi$). It may occur in the highest excited state or in any of the lower excited as well (see Fig. 3a).[36] Usually, at high temperatures, this is the most dominant mode of relaxation because of the considerable phonon energy needed for this excitation, except for the cases where the gap between the m_J levels is very small. The inelastic dispersion of phonons governs the Raman process, and hence the energy limitation present in the Orbach process is not present in the Raman process.

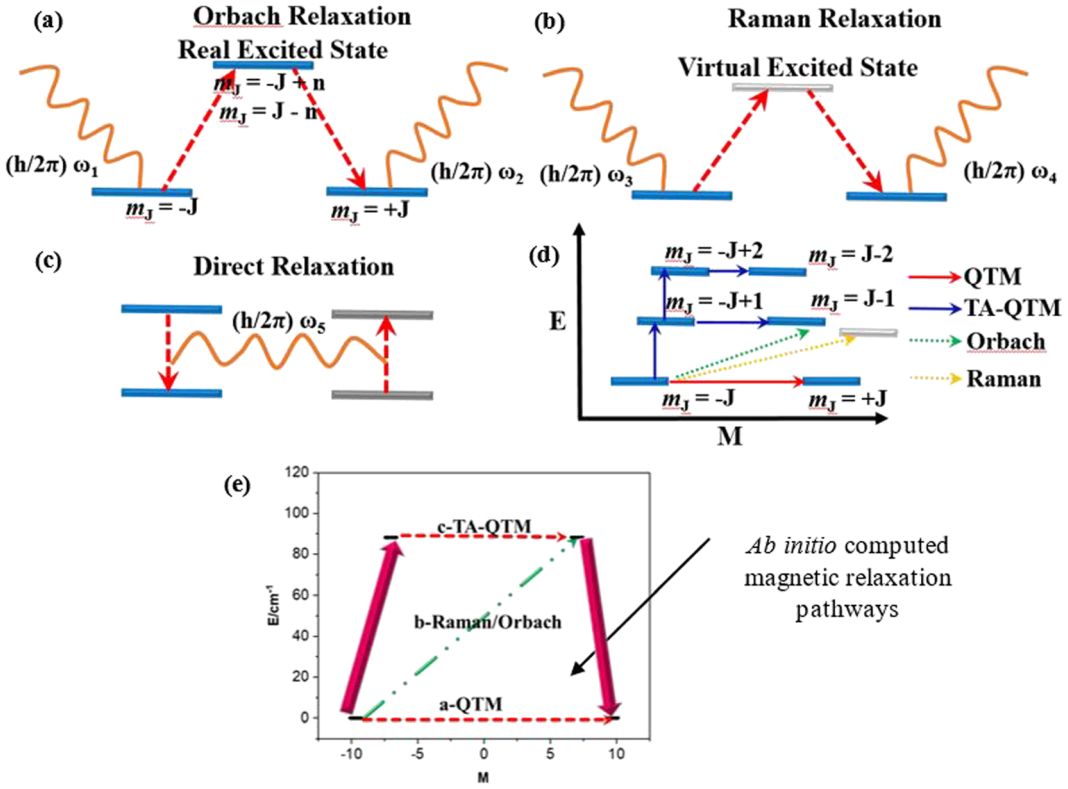

Fig. 3 (a) Schematic representation of Orbach, (b) Raman and (c) direct magnetization relaxation mechanisms. (d) A combination of several relaxation mechanisms, including QTM and TA-QTM, for a part of double-well energy potential. (e) Represents the *ab initio* computed magnetic relaxation pathways, the black dash indicates the low-lying Kramers doublets (KDs), the arrows represent the various pathways and the a, b, and c are the magnitude of transition moment from one state to another. This scheme is used as a reference for all other figures discussed in this work.

A phonon $h\omega_3/2\pi$ is absorbed by the molecule, which then enters a virtual excited state and emits another phonon $h\omega_4/2\pi$ (Fig. 3b).[36] The energy difference between the two phonons in the ground state corresponds to the energy difference between the m_J sub-levels.

On the other hand, the direct process (Fig. 3c) is a single phonon magnetisation relaxation process that directly emits a phonon ($h\omega_5/2\pi$), which corresponds to the energy difference between the m_J sublevels in the ground state.[37] In contrast to these spin–phonon relaxation processes, QTM occurs between the ground m_J levels, frequently found at low temperatures. However, the relaxation pathway could be a combination of processes, with absorbing phonons populating excited states, followed by QTM between $\pm m_J$ states of the same energy (but different sign) and relaxing to the ground sublevel. Thermally Assisted Quantum Tunneling of the Magnetisation, or TA-QTM, is the name given to this coupled mechanism (Fig. 3d).[8] It is worth noting that QTM and direct processes are often most significant at low temperatures, Orbach at high temperatures, and TA-QTM at intermediate temperatures. On the other hand, the Raman process can emerge at any temperature. Among these processes, both QTM and TA-QTM are shortcuts for the relaxation process, which diminishes the effective energy barrier and influences the value of blocking temperature and the relaxation time.[38] Therefore, it is important to understand the origin of QTM, and the strategy to quench QTM in SMMs needs to be explored.[39]

1.2. Origin of QTM

Contrary to the macroscopic particle, the quantum systems can have a double existence at a time; their occupancy is possible in two different states at a time for the particular system. Let us consider a macroscopic classical system (a system having a significant mass m) placed in a double-well; this system can exist at point A at one particular time. To proceed to state B, it needs to overcome the energy barrier ΔE. Unlike this system, quantum systems such as the spin of an electron can simultaneously exist at two states as they can tunnel between them without a barrier, defined as quantum tunnelling. Since the concept of SMM originates from the electrons, which are microscopic, this is related to one of the basic principles for the relaxation of magnetization and predominantly works for all single-molecule magnets. For the transition metal SMMs, m_s and lanthanide m_J states determine the magnetic relaxations originating from the molecular origin (Fig. 1). To have a frozen magnetic state, the m_s and m_J states need to be stable and not flip to the other degenerate state. As QTM is inherent to such systems, one way to annihilate QTM is by lifting these states' degeneracy.[38]

It is well known that the tunnelling probability scales exponentially with the barrier height and the particle mass. The tunnelling probability depends on the interaction of the two wave functions corresponding to these two states (the degenerate states for the Kramers ions). If there is a significant overlap between these two-wave functions, the two levels will split further into two degenerate levels, and the gap between them gives tunnel splitting. Landau, Zener, and Stuckelberg first discussed the non-adiabatic transition between two states, and the tunnelling probability P for an avoided energy level crossing when the field is swept along the z-direction (H_z) at a constant rate is given as[40–43]

$$P = 1 - \exp\left[-\frac{\pi\Delta_{m,m'}{}^2}{2\hbar g_{zz}\mu_B|m-m'|\mu_0 dH_z/dt}\right] \quad (2)$$

Here, $\Delta m,m'$ is the tunnel splitting between the two levels m and m', which are the corresponding states of the avoided level crossing, dH_z/dt is the constant field sweeping rates, μ_B the Bohr magneton, and $\hbar$ is Planck's constant and g_{zz} is the effective g-tensor of the doublet state along the z-direction.

The probability of tunnelling is related to the relative energies of the tunnel splitting and the height of the barrier. The smaller the ratio between the two, the smaller the possibility of observing tunnelling.[38] The QTM consists of two possibilities: direct tunnelling between the two components of the ground doublet, and tunnelling *via* excited states (TA-QTM), which often have larger transverse terms. In an ideal isolated system of Kramers ion with no transverse, intramolecular dipolar or hyperfine interactions and microscopic states without contact with the environment, the QTM can be avoided without any external coupling.[22,44–46] However, in practice, the molecule stays in a crystal lattice. It has been found that coherent tunnelling absorbs energy at a frequency corresponding to the tunnel splitting, leading to magnetization relaxation.[38] For Lanthanides, the QTM arises because of first-order Zeeman splitting of the doublet states induced by the transversal magnetic field, which is proportional to the matrix element of the transversal magnetic moment between the two doublet states.[47,48] Hence, for the Lanthanide complexes, the matrix elements of the transversal component and the tunnelling gap define the magnetic relaxation mechanisms. The calculated blocking barrier can be defined as the shortest path where these values are the largest. A general schematic representation for the *ab initio* computed magnetic relaxation pathways is provided in Fig. 3e.[47]

In this feature article, we explored the factors affecting and causing QTM in lanthanide-based molecular magnets and viable approaches developed over time to quench this process partially or completely. The different approaches to quench QTM at zero-field have been classified into five sections (i) introducing the symmetry through chemical modification or isotopic enrichment by utilizing nuclear spin-free metal ions in Ln SIMs, (ii) inducing a super-exchange interaction by incorporating additional paramagnetic species in the cluster aggregation, (iii) inducing a direct-exchange between lanthanides and/or a paramagnetic species (iv) *via* external stimuli such as an electric field or pressure and (v) an unconventional approach of employing toroidal magnetic states.

2. Various strategies to quench QTM in Ln SMMs

2.1. Quenching the QTM in Ln SIM by employing molecular symmetry

For the single-ion magnets (SIMs), particularly for lanthanides, the magnetic anisotropy originated due to the interaction of lanthanide ions with the ligand field environment, which splits the crystal field into various m_J states, and the splitting of the m_J levels correlates to the strength of anisotropy.[27,49] The symmetry around the Ln^{III} centres plays the most significant role in determining the anisotropy of the corresponding Ln^{III} ion. The transverse anisotropy in lanthanides is significant as it exists even in strongly axial systems as higher-order terms except models possessing cylindrical symmetry such as $\{Dy(OH)_2\}^{+50}$ and $[DyO]^+$.[51] The crystal field Hamiltonian acts on the ground atomic multiplet and splits into $2J+1$ states pairwise degenerate for half-integer states. The crystal field acting on an electronic shell, nl of a lanthanide ion, is given by eqn (3).[52]

$$H_{CF} = \sum_{k,q} B_k^q O_k^q \quad (3)$$

where O_k^q = extended stevens operator (ESO) and k is rank = 2,4,6, and q is a component of the Irreducible Tensor Operators (ITOs)= $+k$, $+k$-1 $\cdots$ $-k$ + 1,$-k$) and B_k^q = crystal field parameters of rank = 2,4,6 for nl = 4f Also here q = 0 represents axial terms whereas $q \neq 0$ represents equatorial terms. As shown earlier, higher-order axial symmetry (with strong axial ligation) quenches the QTM. For example, SMM with a five-fold rotation axis has only $B_k^{\pm 5}$ transverse CF parameter boosting its performance.

The presence of ligand field in the equatorial plane for Ln^{III} SMMs often yields a transverse crystal field, represented by $q \neq 0$, which would couple different m_J states and alter their energy levels.[52,53] For non-Kramers ion, this generates a tunnel splitting (Δ_{tun}), same as that of the Landau–Zener formula. The magnitude is often obtained from *ab initio* calculations and gives a clear picture of the nature of tunnelling. A magnitude smaller than 10^{-6} cm^{-1} usually suggests that Δ_{tun} is absent or negligible.[47,54] For Kramers ion, the internal transverse magnetic field that arises due to various factors, as discussed above, yields a finite tunnelling probability given by the following equation.[47,54]

$$2\Delta_{tun} = \mu_B\left[g_x{}^2H_x{}^2 + g_y{}^2H_y{}^2\right]^{\frac{1}{2}} \quad (4)$$

where g_x and g_y are transversal g factors of the doublet, corresponding to perpendicular directions to its main magnetic axis. H_x and H_y are respective components of the magnetic field. Any values which are greater than 10^{-2} μ_B is considered significant, and the larger the value, the greater the tunnelling probability between the state.[54] From this equation, it is clear that to suppress the QTM, it is important to stabilize large $|m_J|$ as their ground state. Earlier studies and reviews have demonstrated that quenching of QTM results from smaller transverse fields and larger axial

fields, and this occurs when the charge distribution surrounding Ln^{III} ions exhibits C_n ($n \geq 7$), C_{5h}/D_{5h} (for which the symmetry axis is five-fold, *i.e.* C_5), S_8/D_{4d}, and S_{12}/D_{6d} symmetry.[28] However, it is impossible to find the exact crystallographic symmetry containing these point groups, but a pseudo-point group containing only the first coordination sphere serves the purpose. Although this is approximate and strongly depends on the nature of the ligands and their associated charge distributions, this works out well for a qualitative understanding of the underlying physics. The CF parameters obtained from *ab initio* calculations are semi-quantitative and often yield an in-depth picture of the relaxation mechanism.[55,56]

For the oblate Dy^{III} ion, a linear or pseudo linear or $D_{4h}/D_{5h}/D_{6h}$ {for example $[Dy(O^tBu)_2(Phpy)_4][BPh_4]$(**1**)($D_{4h}$),[57] $[Dy(O^tBu)_2(py)_5][BPh_4]$(**2**)($D_{5h}$),[58] $[Dy(LN_6)(Ph_3SiO)_2](BPh_4)]$(**3**)($D_{6h}$)}[59] geometry offers a larger blocking barrier. These three complexes are structurally analogous as they have an $\{O_2N_n, n = 4, 5, 6\}$ pocket around the Dy^{III} ion, with the oxygen atoms in the axial position and nitrogen atoms in the equatorial position. Very large U_{eff} barriers have been observed for all three complexes (ranging from 781 cm^{-1} to 1442 cm^{-1}, see Fig. 4). Despite having very large U_{eff} values, the D_{4h} and D_{6h} complexes were found to exhibit only a moderate T_B^{hys} of $\sim$5 K(@0.001 T s^{-1}), whereas the D_{5h} complexes showed a T_B^{hys} value of 8.8 K (@0.0012 T s^{-1}) (T_B^{FZ} of 14 K). The *ab initio* computed magnetic relaxation dynamics plot reveals that for D_{4h} and D_{5h} complexes, the relaxation occurs *via* the 4th excited state. For complex possessing D_{6h} symmetry, it was found to occur *via* the 2nd excited state (see Fig. 4). This is consistent with the above analogy drawn based on point group symmetry. Further *ab initio* calculations on the D_{4h} molecule reveal a significant B_4^4 term, while for the D_{6h} molecule, additional terms such as B_6^6 appear, enabling larger tunnelling probability. For comparison, the available B_2^2 values for these three complexes are 0.12, 0.06, and 0.55 cm^{-1} for D_{4h}, D_{5h}, and D_{6h}, respectively.[57–59] These three values corresponding to each symmetry reflect the computed QTM probability and the barrier for the magnetization reversal. However, the T_B values for these three complexes are not directly related to the U_{eff} values and suggest that these are controlled by spin–phonon mechanisms, among others, as shown in several lanthanide SMMs.[60–63] A similar D_{5h} air-stable complex $[Dy(H_2O)_5(PNR)_2]$ (PNR = ^{tert}BuPO(NH^{i}Pr)$_2$) (**4-Dy**)(D_{5h}) (Fig. 5a) has been reported by us with a T_B^{hys} value of 12 K (@0.0018 T s^{-1}) (T_B^{FZ} of 14 K, U_{eff} of 511 cm^{-1}), which is one of the first molecules of this type reported with a very large T_B value.[64] As reported by us, analogues $[Tb(H_2O)_5(PNR)_2]$ (**4-Tb**) and $[Ho(H_2O)_5(PNR)_2]$ (**4-Ho**) having pseudo D_{5h} geometry and oblate electron density for the highest m_J levels, yield contrasting magnetic behaviour with **4-Ho** exhibiting U_{eff} of 247 K with T_B^{hys} of 4 K (@0.027 T s^{-1}) and **4-Tb** exhibiting strong quantum tunnelling of magnetization between the ground state.[65] *Ab initio* calculations on these two complexes along with several models (**4-Ln$^{model1-3}$**, Ln = Ho, Tb) (Fig. 5) where the equatorial water molecules are removed sequentially reveal that the presence of strong axial ligand and moderate equatorial ligand is sufficient to quench QTM for Dy(III) as well for Ho(III) but not for Tb(III). Particularly model studies show that Tb(III), having extreme oblicity, has very less tolerance for the equatorial ligand, and this is followed by Ho(III) and Dy(III) (Fig. 5).[65]

Bendix *et al.* reported a chemically unaltered dysprosium complex with a non-linear (C_4) to pseudo-linear (D_{4d}) alteration in crystal field symmetry for two complexes ($[NEt_4][Dy\{Pt(SAc)_4\}_2]$ (**5**) and $[PPh_4][Dy\{Pt(SAc)_4\}_2]$(**6**).[66] In contrast to the low-symmetric **5**, it appears that the higher symmetry in **6** causes a three times

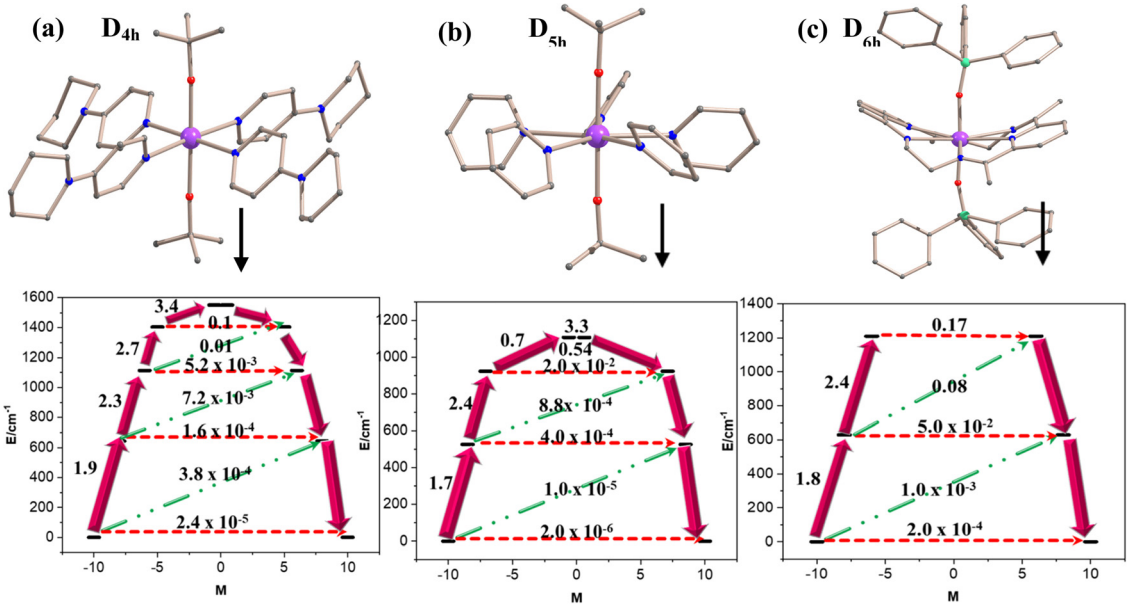

Fig. 4 The *ab initio* computed relaxation dynamics for the (a) D_{4h} (**1**), (b) D_{5h}(**2**) and (c) D_{6h}(**3**) complexes along with the crystal structures. The representation for the plot follows the generalized scheme provided in Fig. 3e. Color code, Purple = Dy, Red = O, Grey = C, Blue = N. Reproduced from ref. 57–59 with permission from [John Wiley and Sons], copyright [2021], [2016] and [2019], respectively.

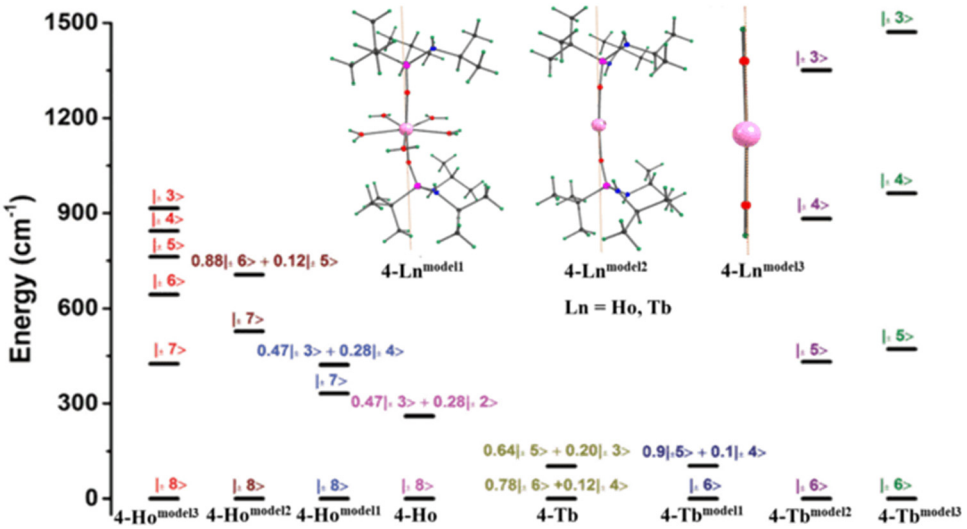

Fig. 5 Variation in the energy splitting of the low lying pseudo-doublets for the complexes **4-Ho** and **4-Tb** and their modelled complexes. Reproduced from ref. 65 with permission from [Royal Society of Chemistry], copyright [2018]

reduction in the ground state tunnel splitting. The off-diagonal B_4^4 CF parameter minimisation reduces the value of the perpendicular component of the ground state *g*-tensor, which in turn, reduces the value of the tunnelling splitting by three folds, nicely demonstrating, using experimental methods, the role of point group symmetry in controlling the CF parameters, which in turn affect the QTM values.

For the Tb^{III} ion with a pseudo D_{4d} symmetry with eight nitrogen atoms coordinated as in $[Pc_2Ln]^-$ TBA^+ (**7**)[25] complex, the largest $m_J = \pm 6$ is stabilised as the ground state with a large crystal field splitting. This was found to show slow magnetic relaxation with barrier height $U_{eff} = 230\ cm^{-1}$, and the QTM is suppressed, as evidenced by the obtained CF parameters ($B_2^0 = -5.05\ cm^{-1}$, $B_2^n = 0.8\ cm^{-1}$ to $3.6\ cm^{-1}$).[67]

The prolate ion, such as Er^{III}, yields better SIMs with trigonal pyramidal pseudo C_{3v} symmetry (having no axial ligation) compared to the other geometries.[68] We extensively studied various Er^{III} SIMs by varying different symmetries and compared the respective Dy^{III} SIM in C_{3v} *vs.* D_{3h} symmetry. The three-coordinate C_{3v} symmetry ($[Ln^{III}(N(SiMe_3)_2)_3]$ (LnN_3 motif where Ln = Er (**8-Er**), Dy (**8-Dy**)) results in $m_J = \pm 15/2$ for the prolate Er^{III} whereas this is reversed for the five-coordinate D_{3h} ($[Ln^{III}(NHPh^iPr_2)_3(THF)_2]$ (LnN_3O_2 motif where Ln = Er (**9-Er**), Dy (**9-Dy**)), for which oblate Dy^{III} shows $m_J = \pm 15/2$ ground state (see Fig. 6).[69] For the C_{3v} symmetry with trigonal pyramidal geometry and absence of any axial ligands offers a strong equatorial field with ground state Ising anisotropy ($g_{xx} = g_{yy} =$ 0.00 and $g_{zz} = 17.877$), whereas for the trigonal bipyramidal D_{3h} symmetry, two of the axial ligand field reverse the m_J ($\pm$ 1/2) states for the Er^{III} ion. Hence for the C_{3v} symmetry structure, the Er^{III} ion yields better SIM characteristics, while for the Dy^{III} ion, D_{3h} symmetry is better suited. Here the presence of axial ligands in D_{3h} and the absence of C_{3v} leads to such results, however a D_{3h} symmetry without any axial ligands will be best suited for prolate ions. Moving from tri-coordinated trigonal planar (QTM probability $\sim 10^{-4}$) to four coordinated vacant-TBP (QTM probability $\sim 10^{-3}$) and tetrahedral (Td) (QTM probability ~ 0.18) for the complex $[Li(THF)_4][Er\{N(SiMe_3)_2\}_3Cl]\cdot$ 2THF(vacant-TBP-**10**, Td-**11**), the QTM at the ground state found to worsen.[70] This further confirms that the presence of a non-planar or axial ligand field is making the Er^{III} SIMs poorer. It is worth mentioning that going from D_{4h} to D_{3h}, the SIM characteristics are poorer for the Dy^{III} ion as reflected in the *ab initio* calculated data.[70]

The lanthanoarenes are the best SIMs reported with Dy ($[Dy(Cp^{ttt})_2][B(C_6F_5)_4]$ ({Cp^{ttt} = $C_5H_2{}^tBu_3$-1,2,4}, **12**,[71] Fig. 7), $[(Cp^{iPr5})Dy(Cp^*)]^+(Cp^{iPr}= C_5{}^iPr_5)$ (**13**),[10] $[Dy(Cp^{iPr4R})_2]^+$ (R = H (**14**), Me (**15**), Et (**16**), iPr (**17**)),[72] Tb $[Ln(Cp^{iPr5})_2]^0$(**18-Tb**)[73] and Er ($[Er(COT)_2]^-$)(**19**)[74,75] centres in their different oxidation states with different arene rings where the size of the arene rings varies from 5 and 8 with the corresponding pseudo symmetry varying from D_{5d} to D_{8d}. Compared to the D_{nh} symmetry, in the Dysprocene organometallic magnets, the U_{eff} is found to be in the range of $\sim 1200\ cm^{-1}$ $\sim 1500\ cm^{-1}$, with the T_B^{hys} of 52 K to 80 K has been achieved. It is worth noting that any distortion in the equatorial plane can lead to non-zero transverse crystal field parameters and thus induce the QTM. Certainly, a complete linear Ln^{III} complex without any equatorial ligand field or an equatorial ligand field with cylindrical symmetry will result in better SIMs and will likely result in record-breaking U_{eff}/T_B values. Even in the organometallic Lanthanoarene systems, if the symmetry is reduced, this results in less performant SIMs, and this is witnessed in recently reported *in silico* designed corannulene-based Dy^{III} SIMs such as ($[(\eta^5$-corannulene)$Dy(C_nH_n)]$ n = 5, 6; **20**),[76] where due to the presence of corannulene, the symmetry around the Dy^{III} centre has been reduced compared to the lanthanoarenes, and this results in a comparatively lesser U_{cal} value for the corannulene based Dy^{III} SIMs (U_{cal} = 599 to 919 cm^{-1}) compared to the complexes **12–17**.

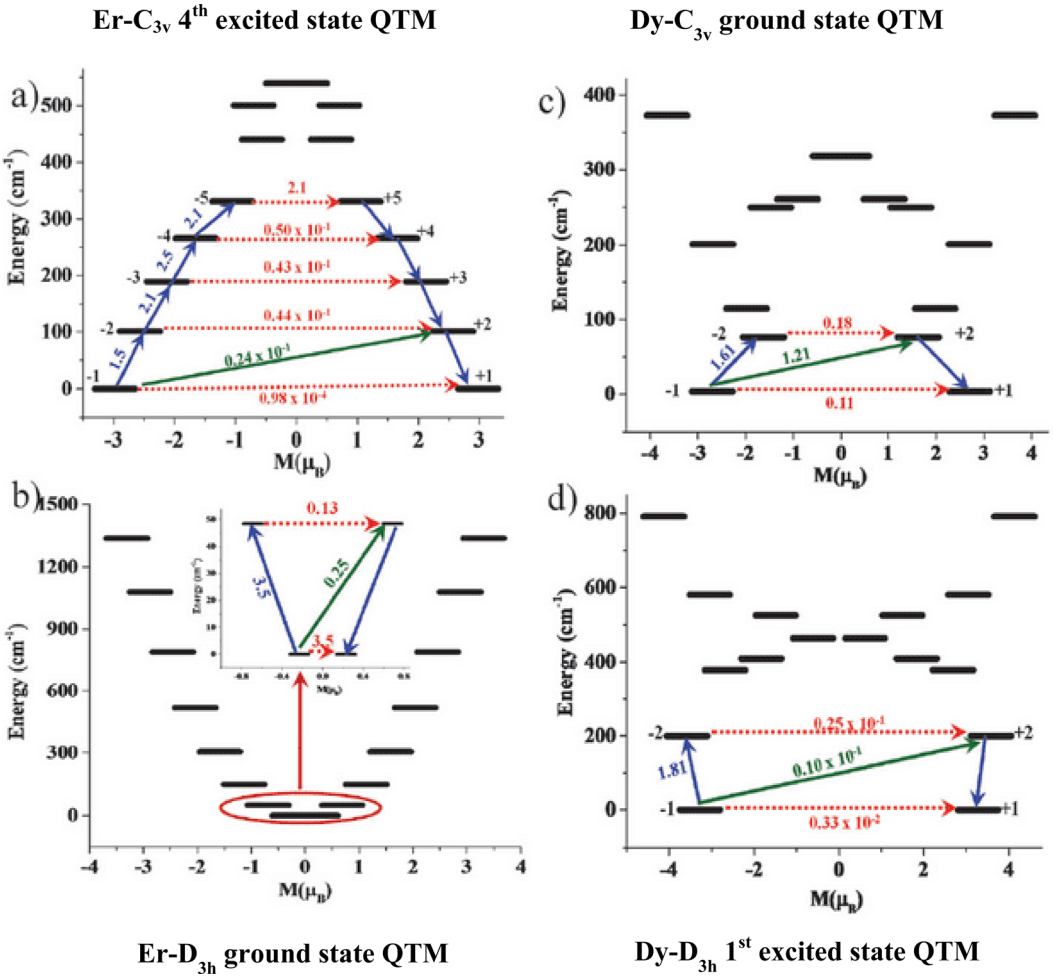

Fig. 6 The *ab initio* computed magnetization blocking barrier for all four complexes: (a) **8-Er** (b) **8-Dy**, (c) **9-Er** and (d) **9-Dy**. The representation of magnetic relaxation dynamics plots follows the generalized scheme provided in Fig. 3e. Reproduced from ref. 69 with permission from [Royal Society of Chemistry], copyright [2014].

As discussed above, the intermolecular and hyperfine interactions are thought to be one of the reasons behind the quantum tunnelling process; another alternative to overcome this is by inducing dilution or incorporating different isotopes into the matrix of the existing complex, which can suppress these two phenomena. This approach has been beautifully summarised for the [Dy(tta)$_3$(L)] (**22-Dy**), (where L = 4,5-bis(propylthio)-tetrathiafulvalene-2-(2-pyridyl)benzimidazole-methyl-2-pyridine) complex. The incorporation of ^{164}Dy (I = 0) in place of ^{161}Dy (I = 5/2) for the above complex in the diluted matrix leads to the opening of the hysteresis loop at the zero-field (see Fig. 8). The ^{161}Dy has a hyperfine constant of −109.5(22) MHz, which helps to fasten the QTM process.[77–80] The same has been performed by taking the Yb analogue ([Yb(tta)$_3$(L)] **22-Yb**). At the lowest studied temperatures, for ^{174}Yb@Y(I = 0), the Raman process dominates the relaxation mechanism, whereas, for ^{173}Yb@Y (I = 5/2), the QTM governs the relaxation process.[81]

Another strategy which is very less explored is the unusual oxidation state of the low symmetry complexes in lanthanides. Recently, the anisotropy and the barrier heights of lanthanides in their +2 oxidation state have been explored by Ungur *et al.* computationally, which shows a record high U_{cal} value of >2000 cm^{-1} for the [Tb^{II}–O](**21**) model complex.[82] In this model system, as Tb^{II} has a similar electron density to the Dy^{III} ion, they tend to be superior. More importantly, despite a weaker ligand field due to reduced charge on the lanthanide metal ions, these models yielded better SIMs due to significant quenching of QTM. This has been witnessed experimentally in the complex **18-Tb** (described above) reported by Long *et al.*, possessing a U_{eff} barrier of 1205 cm^{-1} with a T_B^{hys} value of 52 K, and these parameters are the highest witnessed for any Tb-based SMMs. The ^{159}Tb nucleus in a neutral [Tb(Cp^{iPr5})$_2$](**18-Tb**)[73] single-molecule magnet (SMM), which displays an abnormally long magnetization relaxation time, has been examined by Park *et al.*, utilising CASSCF methods.[83] They have demonstrated that the $4f^8(6s,5d_{z2})^1$, $4f^8(5d_{x2-y2})^1$, and $4f^8(5d_{xy})^1$ configuration are the lowest energy states According to the multiconfigurational approach estimated hyperfine interaction parameters and electronic–nuclear spectrum, the hyperfine interaction is roughly an order of magnitude larger than that of [Tb^{III}Pc$_2$] (7) SMMs. Due to the occupation of the 6s and 5d orbitals, there is a significant Fermi contact interaction between the Tb

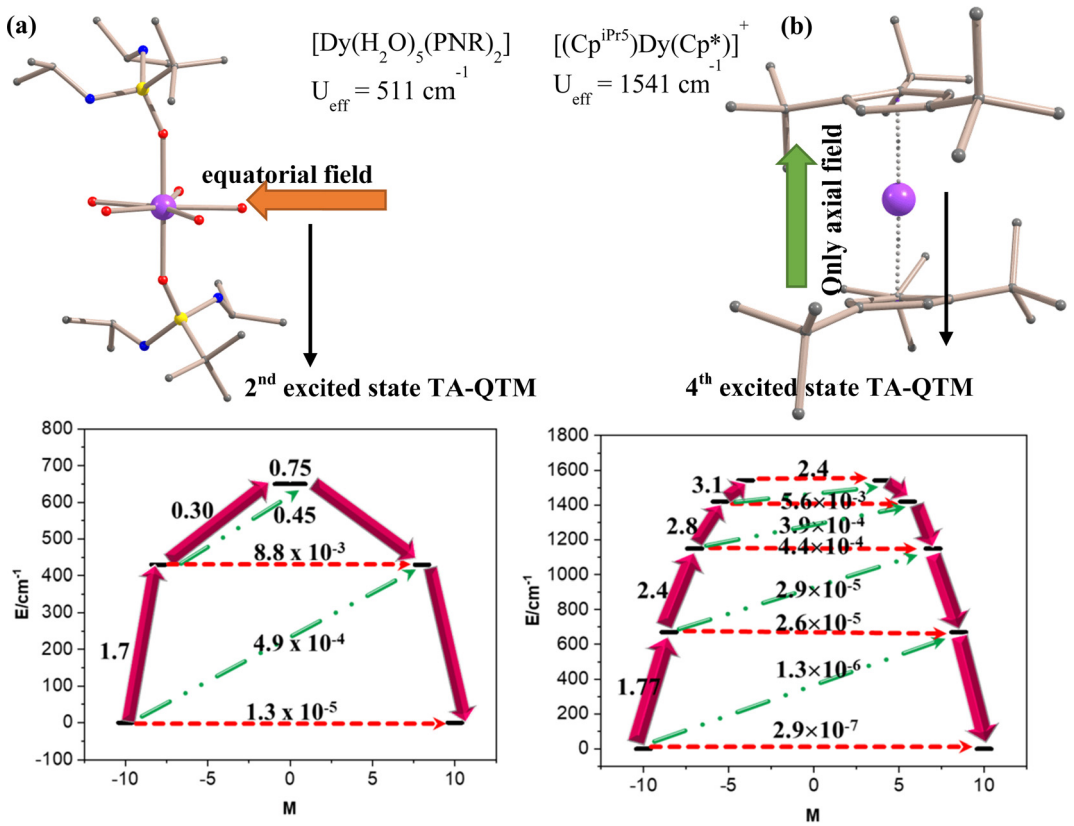

Fig. 7 (a) Molecular structure of Dy(III) pseudo D_{5h} complex (**4-Dy**) and (b) pseudo liner complexes $[Dy(Cp^{ttt})_2]^+$(**12**) along with the *ab initio* computed magnetic relaxation pathways. The representation of magnetic relaxation dynamics plots follow the generalized scheme provided in Fig. 3e. The H atoms and solvent molecules are omitted for clarity. Purple Dy, Red O, gray C. Reproduced from ref. 64 and 71 with permission from [Royal Society of Chemistry], copyright [2016] and [Springer Nature], copyright [2017], respectively.

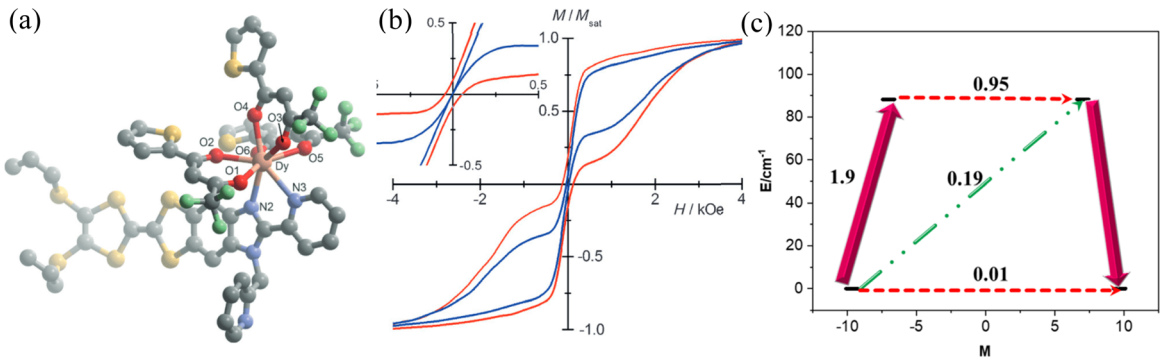

Fig. 8 (a) Molecular structure of complex **22-Dy** (H atoms and solvent molecules are omitted for clarity). Green F, yellow S, gray C. (b) Normalized magnetic hysteresis loops measured at 0.46 K on the diluted forms of ^{161}Dy (I = 5/2, in blue) and ^{164}Dy (I = 0, in red). (c) The *ab initio* computed magnetic relaxation dynamics plots for **22-Dy** which follow the generalized scheme provided in Fig. 3e. Reproduced from ref. 78 with permission from [John Wiley and Sons], copyright [2015].

nuclear spin and the density of electron spins at the nucleus. The strong uniaxial magnetic anisotropy causes the electronic Kramers doublet to have substantial excitation energy of 311 cm^{-1}, which is significantly higher than the splitting of the electronic–nuclear levels for the Tb nuclear spin (I = 3/2).[83] A recent report by Popov *et al.* illustrates the 4f-shell and valence magnetism (FV-magnetism) may show magnetic bistability up to unexpectedly high temperatures for such Tb^{II} system depicting its importance.[84]

2.2. Quenching the QTM using super-exchange interaction

Contrary to the SIMs, in a multinuclear system, the origin of magnetic relaxation does not depend fully on the single ion anisotropic behaviour of the paramagnetic metal centre; rather,

it depends on the anisotropy of the exchange coupled states.[85–87] For an exchange-coupled system, the paramagnetic units (m_S or m_J) are now coupled with each other. A pictorial representation has been provided in Fig. 9b by comparing the SIM QTM (in Fig. 9a) behaviour *vs.* exchange coupled QTM behaviour. In the multinuclear system, if a suitable exchange coupling is present, this act as an internal static magnetic field and can mimic an external applied magnetic field and quench the QTM effectively. All these quenching denoted here are at zero magnetic fields. It is important to note that while the exchange coupling constant quenches the QTM at zero-field, the tunnelling can still occur at higher fields if the exchange coupled states are accessible *via* the resonant tunnelling process. It is important to target extremely large exchange interactions to avoid such effects.

On the basis of the obtained CF states, the exchange levels for a Ln^{III} paramagnetic system are given by the following Hamiltonian (in the strong-exchange limit),

$$\hat{H} = \hat{H}_{CF} + \hat{H}'_{CF} + \hat{H}_{ex} \quad (5)$$

$$\hat{H}'_{CF} = \sum_{i=1,2} \cdot \sum_{k=2}^{6} \cdot \sum_{q=-k}^{k} \mathcal{I}_{kq00} \frac{O_k^q(\hat{J}_i)\hat{I}}{O_k^0(J)} \quad (6)$$

$$\hat{H}_{ex} = \sum_{i=1,2} \cdot \sum_{k=1}^{6} \cdot \sum_{q,q'}^{k} \mathcal{I}_{kq1q'} \frac{O_k^q(\hat{J}_i)\hat{S}}{O_k^0(J)S} \quad (7)$$

where $\hat{H}_{CF}$ and $\hat{H}'_{CF}$ are the contribution to the local CF splitting, and CF arising from the electron delocalization between Ln^{III} ions and neighbouring spin, and $\hat{H}_{ex}$ describes the exchange interaction between them; J_{kq00} (even k) and $J_{kq1q'}$ (odd k) are exchange parameters with rank k and projection $|q| \leq k$; $\hat{I}$ and $\hat{S}$ is the unit and spin operators of the paramagnetic species (excluding its anisotropy, if any), respectively.[88] The presence of exchange coupling splits the states further, leading to exchange-coupled states, and this splitting lifts the degeneracy, leading to the quenching of the QTM levels (Fig. 9b).

To increase this coupling, one needs to understand the mechanism of exchange coupling between the metal centres, whether it is coupled *via* a radical bridge (direct exchange) or a diamagnetic hetero bridge (super-exchange). The nature and extent of magnetic coupling depend on the arrangement of orbitals and the degree of overlap between them. With this, the unpaired electrons and the vacant orbitals on the metal centres determine the extent of charge transfer from one centre to another. Two of the most important factors which control the sign and strength of J_s are the degree of orbital overlap and the charge transfer. Stronger orbital overlaps contribute toward the antiferromagnetic coupling part, whereas contribution to ferromagnetic coupling arises due to charge transfer phenomena. Our group has developed several magneto-structural correlations to gain insight into the nature of exchange coupling in {3d–4f} and {radical-4f} pairs (see Fig. 10).[89,90] Employing DFT and *ab initio* methods, the overlap between the SOMOs, the mechanism of spin distribution (polarisation and delocalisation), and the nature of charge transfer were established by us and others.[71] The exchange contributes from the intramolecular Dy–Dy coupling and the dipolar coupling between the two centres. The nature of the interaction, whether ferro or antiferro, is often subjected to the Dy–X–Dy angle (X being the bridging atom/group).

First, we will discuss the super-exchange in 4f–4f and 3d/4d–4f complexes where O, N, and halide ions bridge the metal ions. Although 4f–4f interactions are weak, the non-negligible magnetic exchange interaction between the Dy–Dy centres has gained attention for quenching QTM.[91] This exchange is generally small and is in the range of 0.01–7 cm^{-1}.[92–94] However, such exchange plays a crucial role in determining the mode of magnetic relaxation and the performance of the SMMs. We have reported a vast example of such dimers, where a negligible magnetic exchange leads to the controlling of relaxation contributed from the single Dy^{III} centre, and a comparatively stronger exchange leads to the relaxation occurring from the exchange coupled states.[95–100] In this regard, we have proposed an empirical equation by studying several asymmetric Dy_2 (lacking inversion symmetry) dimers to determine the U_{eff} barrier for such exchanged coupled states, as follows,[101]

$$U_{caleff} = \left[\frac{U_{cal1}}{(\mathrm{QTM\ or\ TA-QTM}) \times 10^3} + \frac{U_{cal2}}{(\mathrm{QTM\ or\ TA-QTM}) \times 10^3}\right] + 15J \quad (8)$$

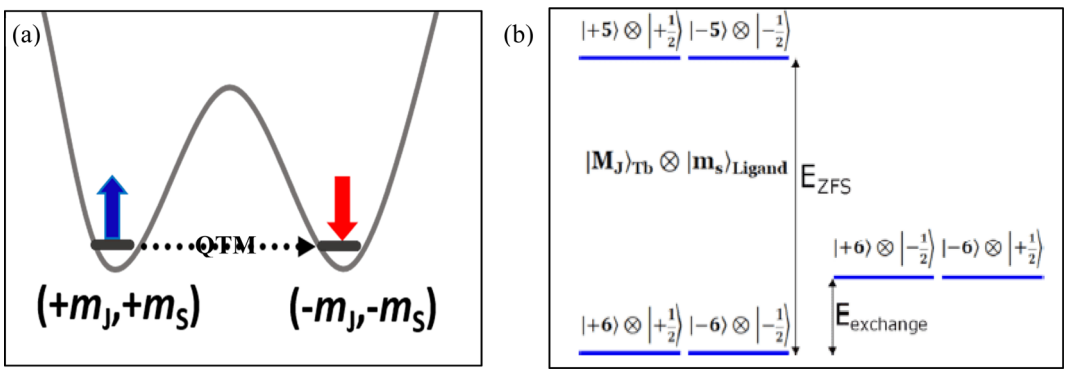

Fig. 9 (a) A schematic comparison of magnetic states flipping in SIMs *vs.* (b) the exchanged coupled system, *i.e.* exchange coupling between m_J level and ligand m_S levels. Reproduced from ref. 67 with permission from [American Chemical Society], copyright [2019].

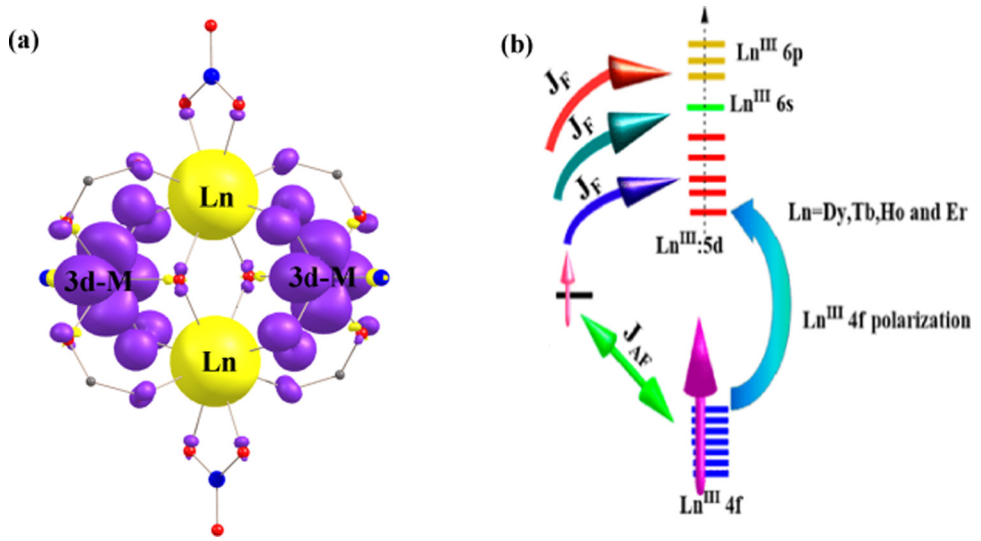

Fig. 10 (a) Representation of the orbital overlaps of the Ln^{III} ions with the transition metal ion and (b) the exchange coupling mechanism. Reproduced from ref. 119 and 89 with permission from [Royal Society of Chemistry], copyright [2021] and [American Chemical Society], copyright [2016].

where U_{cal1} and U_{cal2} are the *ab initio* CASSCF/RASSI-SO/SINGLE_-ANISO calculated blocking barrier for Dy1 and Dy2 centres, respectively, and J is the exchange coupling. This proposed equation yielded a good numerical estimate of barrier height for most of the 31 non-centrosymmetric Dy_2 having super-exchange interactions studied, except for complexes where the Raman process is dominant.

However, in endohedral fullerene $Dy_2O@C_{80}$(**23**), the gap between the ferro-antiferromagnetic states is reported to reach as high as -18 cm^{-1}, highlighting the importance of structural parameters around the Dy^{III} centres to alter the magnitude of exchange coupling values.[102] For the $Dy_2O@C_{80}$, such a large gap observed leads to quenching of QTM and a substantial T_B^{FZ} value of 11–12 K (T_B^{hys} 6 K 0.0029 Ts^{-1}) (see Fig. 11) despite having antiferromagnetic coupling between two Dy^{III} centres. The non-colinear arrangement of the Dy^{III} anisotropic axes was found to be responsible for the intrinsic SMM characteristics.

In the organometallic multi-decker complexes, moderate to weak exchange coupling between the metal centres also increased the T_B values. Compared to the double-decker analogue of the $[Er(COT)_2]^-$(**19**)[54] complex, the triple-decker $[Er_2(COT'')_3]$(**24**) and quadruple decker $K_2(THF)_4[Er_2(COT)_4]$(**25**) complexes show a T_B^{hys} value of 12 K (14 K in the solution state, sweep rate 0.0022 and 0.0018 T s^{-1}, T_B^{100} 12.5 K and 12.9 K respectively for **24** and **25**) in solid-state which is 4 K higher than the double-decker complex.[75] This is attributed to the exchange coupling between the Er–Er centres with an estimated J of -0.5 cm^{-1} for the Gd analogue of complex **24**.

The magnitude of the exchange reported in the 4f–4f pair is often small due to the deep burial of 4f orbitals, which feebly interacts with the ligand, and therefore, their contribution to

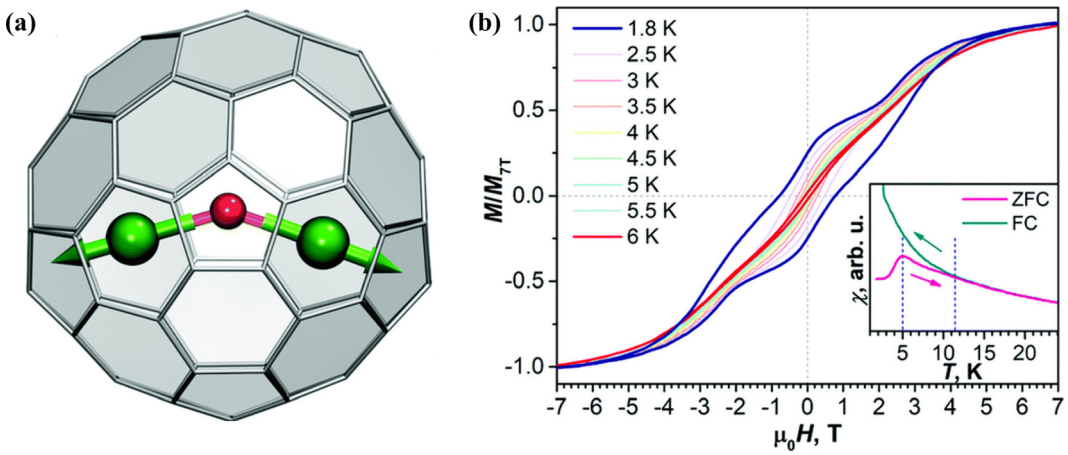

Fig. 11 (a) Molecular structure of complex **23** ($Dy_2O@C_{80}$) and (b) the corresponding magnetic hysteresis plot for complex **23** (ZFC *vs.* FC measured magnetic susceptibility with respect to temperature plot inset). Reproduced from ref. 102 with permission from [Royal Society of Chemistry], copyright [2022].

the super-exchange is often a few cm^{-1}.[93,103] The coupling of lanthanide ions with a paramagnetic transition metal ion, where the 3d/4d electron is exposed, can provide a more considerable interaction between the lanthanide centres.[104–107] Gatteschi and co-workers have pioneered the first generation 3d–4f complexes to study the magnetic properties of Cu^{II}–Gd^{III} complexes.[90,108] Several 3d–4f metal clusters and their magnetic properties have been summarised by many previously; the number of such complexes is quite large; however, in most cases, either the barrier for magnetic reversal is small, or the T_B values are quite small.[106,107,109] The largest U_{eff} for the 3d–4f class of complex is reported with the complex $[Co_2Dy(L^{Br})_2(H_2O)]NO_3$(where L^{Br} = 2,2′, 2″-(((nitrilotris(ethane-2,1-diyl))tris(azanediyl))tris(methylene))tris-(4-bromophenol))(**26**) with U_{eff} 416 cm^{-1}; however, no opening of hysteresis or blocking temperature was observed for the above complex. Hence, a large exchange coupling between the metal ions and the magnetic anisotropy has to be persistent in 3d–4f complexes to achieve better SMM properties.

This has been achieved in the classic examples of 3d–4f butterfly complexes, where two lanthanides and two 3d metal ions form a tetranuclear butterfly core.[110] In the 3d–4f butterfly complexes, a square antiprism geometry around the Ln^{III} centre, with eight O donors from the ligand, makes it suitable to retain the anisotropy around the metal Ln^{III} centres. Murray *et al.* have reported several such complexes where the magnetic anisotropy of 4f ions, in combination with the exchange interaction with the 3d metals, leads to the opening of hysteresis at temperatures above 2 K (T_B^{hys} = 2 K).[110–116] The first butterfly with such a large exchange has been reported with a tetranuclear $\{Cr_2Dy_2\}$(see Fig. 12) core having the molecular formula $[Cr^{III}_2Dy^{III}_2(OMe)_2(O_2CPh)_4(mdea)_2(NO_3)_2]$ (**27-Dy,** see Fig. 5), where mdea = methyldiethanolamine, with an U_{eff} = 54 cm^{-1}.[114] Despite having a very large U_{cal} barrier originating from the single Dy^{III} centres (of the order of 300 cm^{-1}), the overall experimental U_{eff} is found to be small for this complex.[114] A large exchange interaction of J_{SP} (J_{SP} denoted here, the exchange value obtained from the spin projected model) has been observed between the Dy^{III}–Cr^{III} centres, which ranges from −16.7 to −20.3 cm^{-1}, and a blocking temperature T_B^{hys} of 3.5 K (@0.003 Ts^{-1}, T_B^{FZ} = 3.7 K) has been achieved. This is attributed to the magnetic relaxation followed by the exchanged coupled state (see Fig. 12). The relaxation happens from the $8^{th}/7^{th}$ excited exchanged coupled state *via* TA-QTM/Orbach process with a transition probability value of 10^{-3} to 2.1 μ_B. Introducing two F^- and one Cl^- at the 4, 5

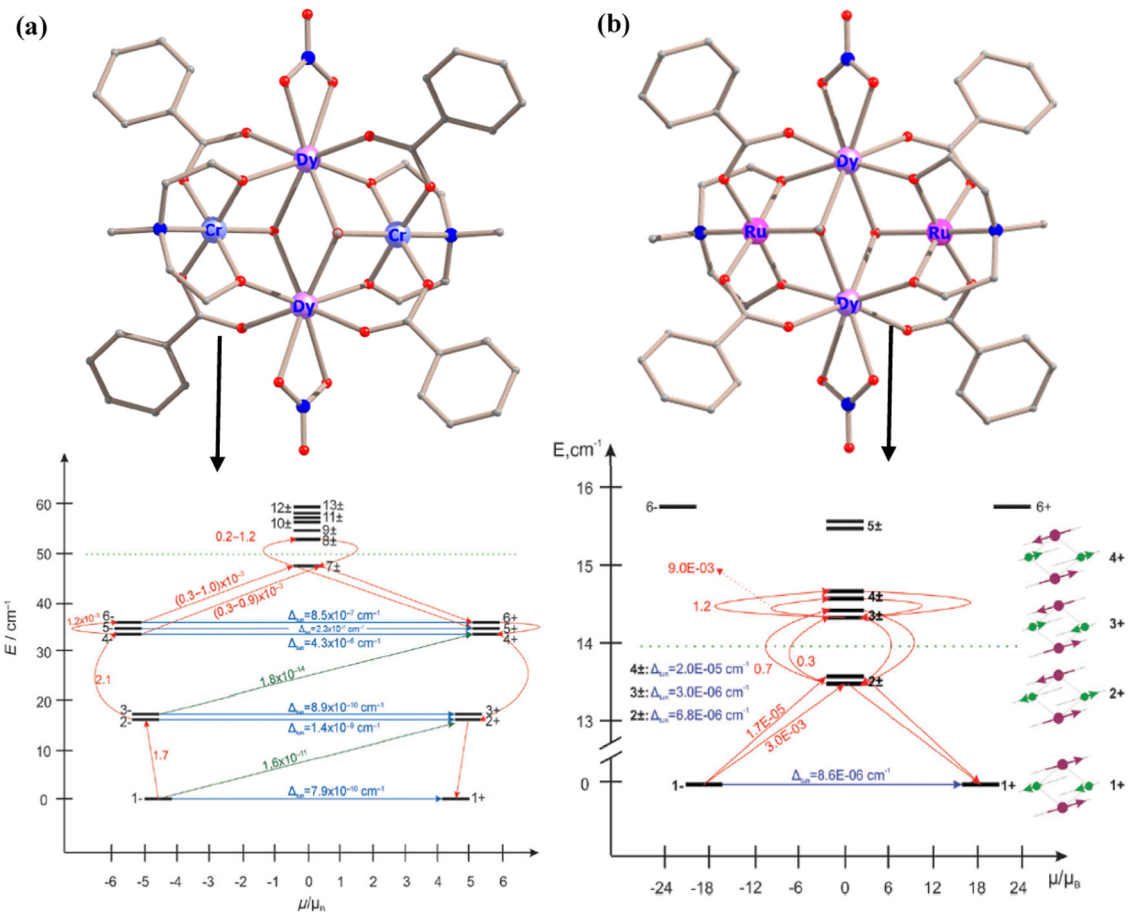

Fig. 12 Low-lying exchange spectrum and the position of the magnetization blocking barrier in M_2Dy_2 (M = Cr(a)(**27-Dy**), Ru(b)(**33-Dy**)) along with the crystal structures. Reproduced from ref. 114 and 116 with permission from [John Wiley and Sons], copyright [2013] and [Royal Society of Chemistry], copyright [2015].

and 2 positions of the benzoate ring, a T_B^{hys} value of 4.7 K has been attained for the same butterfly core $[Cr^{III}_2Dy^{III}_2(OMe)_2(2\text{-Cl},4,5\text{-}FO_2CPh)_4(mdea)_2(NO_3)_2]$(**28-Dy**), with a U_{eff} value of 60 cm^{-1} due to the increased exchange coupling between the two paramagnetic metal centres.[113] Replacing the Dy^{III} by Tb^{III} and Ho^{III} in $[Cr^{III}_2Ln^{III}_2(OMe)_2(O_2CPh)_4(mdea)_2(NO_3)_2]$(**27-Tb**, **27-Ho**)[117] (Ln = Tb, Ho), decreases the T_B^{hys} value to 2.5 K and 1.8 K for **27-Tb** and **27-Ho**, respectively whereas in $[Cr^{III}_2Ln^{III}_2(OMe)_2(2\text{-Cl},4,5\text{-}FO_2CPh)_4(mdea)_2(NO_3)_2]$ (Ln = **28-Tb**, **28-Ho**), T_B^{hys} of 3.5 and 2.4 K has been observed owing to the less anisotropy of the Tb^{III} and Ho^{III} centres compared to the Dy^{III} ion.[113] Replacing the benzoate analogue with acac-(acetylacetonate) in $[Cr^{III}_2Dy^{III}_2(OMe)_2(RN\{(CH_2)_2OH\}_2)_2(acac)_4(NO_3)_2]$[115] (R = Me(**29-Dy**), Et(**30-Dy**), *n*-Bu(**31-Dy**) resulted in a decrease of U_{eff} to 29 cm^{-1} and the T_B^{hys} value to 2.2 K. The decrease in blocking temperature is attributed to the less exchange coupling between the Cr–Dy ($J_{SP-Cr-Dy}$ = −7.14 to −11.8 cm^{-1}).[115] Compared to the benzoate analogue, where there are three μ_3 oxo linkers present between Cr^{III} and Dy^{III}, in the later analogue, only two are present, resulting in a net decrease in J values. In all of these classes of complexes, the mode of magnetic relaxation proceeds *via* Orbach processes, and the overall blocking barrier arises from the exchanged coupled states. Contrary to the paramagnetic Cr^{III} centre, when the isostructural Co^{III} diamagnetic analogue was made by replacing the Cr^{III} with Co^{III} in $[Co^{III}_2Dy^{III}_2(OMe)_2(O_2CPh)_4(Htea)_2(NO_3)_2]$(**32-Dy**), the U_{eff} has increased to 62 cm^{-1}, however, magnetic hysteresis has not been observed above 2 K due to strong quantum tunnelling. This is due to the absence of exchange coupling in $\{Co^{III}_2Dy^{III}_2\}$ (**32-Dy**) analogues.[111] The *acac* analogue with Co^{III} shows a similar trend with no observable hysteresis at the measured temperatures.[118] This clearly illustrates the importance of exchange coupling in quenching QTM. Though the exchange often reduces the overall barrier height, its presence often yields blocking temperature, which is the most important criterion for SMMs. Henceforth, we can conclude that it is advantageous to have paramagnetic metal ions in the cluster aggregation as it more than compensates for reducing single-ion anisotropy in these clusters. Numerous other TM_2Ln_2 butterfly cores with TM = Cr, Mn, Fe, Co, Ni, Cu, Zn, and Ln = Dy, Ho, Tb, Er, Eu, Yb, Nd have been reported by various groups, which were summarised beautifully by Powell *et al.*[110] Replacement of 3d paramagnetic centres with the 4d expected to produce even larger exchange coupling with the Ln^{III} as the 4d orbitals are larger and more diffused in character, which will provide more significant overlap between the magnetic orbitals leading to a prominent exchange. This has been achieved by replacing the Cr^{III} with Ru^{III} in the parent butterfly complex with the molecular formula $[Ru^{III}_2Dy^{III}_2(OMe)_2(O_2CPh)_4(mdea)_2(NO_3)_2]$(**33-Dy**) reported by Murray's group and us.[116,119] However, contrary results were observed, and a lesser exchange was estimated for Ru–Dy (J_{Ru-Dy} = −1.8 to −2.4 cm^{-1}). A closer look at the electronic structure using DFT and *ab initio* calculations reveals that the unpaired electron present in the d_{xy} orbital of the Ru^{III} ion has an unfavourable orientation for strong overlap with 4f orbitals leading to a weaker exchange. While for the Cr^{III} ion having three unpaired electrons in d_{xy}, d_{xz} and d_{yz} orbitals, independent of the cluster topology, there is always one interaction that is strong and sufficient to boost the J values. Compared to complex **27-Dy**, now the magnetic relaxation happens from the 1st/2nd excited state of the exchanged coupled state for complex **33-Dy** (see Fig. 12b). Such a small exchange coupling in **33-Dy** is not sufficient enough to quench the QTM and therefore this complex exhibit hysteresis loop only below 2 K (T_B^{hys} < 2 K).

Besides these examples, there are also several experimental examples where strong coupling between Ln(III) ions leads to quenching of QTM at zero-field. At the same time, the tunnelling was visible at the higher-field, and the field at which the QTM was observed was correlated to the strength of the exchange coupling.[91,120] Further, the role of exchange coupled states interacting with the nuclear spin yielding QTM between entangled states of the electronic and nuclear spin systems are observed where the QTM is shifted to higher field strength depending on the nature of exchange and the magnitude of the hyperfine coupling constants.[121,122]

2.3. Quenching the QTM using direct exchange interaction

Apart from the super-exchange, the second kind of exchange interaction is the direct exchange, and many SMMs with a significant direct exchange coupling between the paramagnetic metal centres, or metal-radical systems, are known to exhibit better SMM characteristics.[89,123] The classic example of phthalocyanine lanthanide double-decker complexes $[LnPc_2]^-.TBA^+$ (Ln = Tb (**7-Tb**), Dy (**7-Dy**), Pc = dianion of phthalocyanine; TBA^+ = $N(C_4H_9)_4^+$) show slow magnetic relaxation with a barrier height of U_{eff} = 230 cm^{-1} and 28 cm^{-1} respectively for **7-Tb** and **7-Dy**.[25,124] The one-electron oxidation of the $[TbPc_2]^-$ to the neutral complex $[TbPc_2]^0$ (**34**) results in an increased barrier height of U_{eff} = 410 cm^{-1}.[125] One unpaired electron (with the spin $S = \frac{1}{2}$) is delocalized (or shared) between the two Pc ligands in neutral $TbPc_2$ SMMs (see Fig. 13). The exchange coupling (J_{ex}) between this radical ligand spin and the Tb magnetic moment doubles the

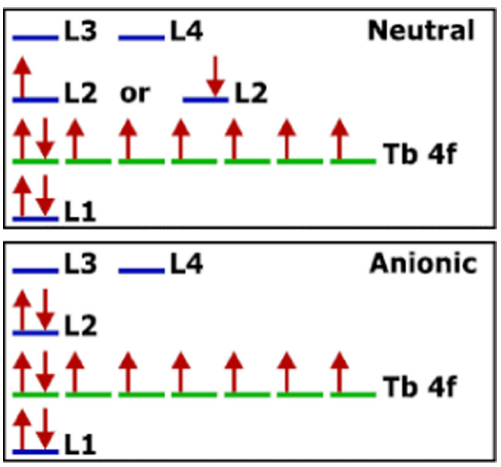

Fig. 13 Schematic illustration of the active space used in the CASSCF calculations for $[Tbpc_2]^-$ and $[Tbpc_2]^0$. Reproduced from ref. 67 with permission from [American Chemical Society], copyright [2019].

number of low-energy states.[67] Furthermore, this extra electron turns neutral [$TbPc_2$] into a Kramers system, ensuring at least twofold degeneracy of all electronic levels enforced by time-reversal symmetry, regardless of ligand field symmetry. Park *et al.* reported that the higher energy levels strongly depend on the ligand type, molecular symmetry, and overall charge of the molecules. Furthermore, ligand distortion and molecular symmetry play a crucial role in transverse CF parameters, which lead to tunnel splitting.[67] The tunnel splitting induces quantum tunnelling of magnetization by itself or by combining with other processes. Compared to the anionic complex [Tb Pc_2]$^-$, for the neutral complex, no tunnel splitting was observed for the ground state as well as excited state quasi-doublets. For the anionic complex, the tunnel splittings of 0.007, 0.090, and 7.969 cm^{-1} have been observed for the ground, 1st, and 2nd excited state quasi doublets. The observed difference in the magnetic properties was attributed to the significant J_{ex} present for the neutral complex compared to the anionic one (J_{ex} = 6.6 to 8.2 cm^{-1}). Moreover, the axial CF parameter (B_2^0 = −5.93 *vs.* −5.05 cm^{-1}) is larger, and the transverse CF parameter (B_2^2 = 0.3 to 0.4 cm^{-1} *vs.* 0.8 to 3.6 cm^{-1}) is small for the latter. Similarly, two-electron oxidation of the [{Pc(OEt)$_8$}$_2$Tb]$^-$ complex to its cationic analogue [{Pc(OEt)$_8$}$_2$-Tb]$^+$(**35**) further enhances the barrier height from 508 cm^{-1} to 550 cm^{-1} because of the existence of unpaired electrons on the two Pc rings.[126–128] Enders, Ishikawa *et al.* showed a further increase in barrier height of up to 588 cm^{-1} in the [(obPc)Tb (Fused-Pc)Tb(obPc)](**36**) complex, where two [Pc_2Tb]^0 units were connected *via* a fused pthalocyanato ligand (see Fig. 15).[129] Two π radicals present in the fused bridge provide an exchange coupling of 2 cm^{-1} between the Tb1-radical1, −0.7 cm^{-1} between Tb1-Tb2, −2.7 cm^{-1} between Tb2-radical2 and −174.3 cm^{-1} between radical1-radical2 (see Fig. 15). These exchanges effectively quench the QTM, a T_B^{FZ} of 18 K was observed for **36**.

Concrete evidence of exchange coupling on magnetic relaxation dynamics was reported by Long *et al.*, which is one of the first of this kind to have very large T_B values.[130] They have reported the dinuclear Tb^{III} complex with the molecular formula {[[$(Me_3Si)_2N]_2$(THF)Tb}$_2$(μ-η$_2$:η$_2$-N_2)$^-$] (**37-Tb**) (Fig. 14 inset), in which the large magnetic exchange between the Tb^{III}-radical found to quench the QTM process at the zero-field making it relax in the thermally activated regime *via* the direct process having (QTM probability ∼10^{-6}) an U_{eff} = 227 cm^{-1}.[130] The magnetic hysteresis has been sustained at 14 K (T_B^{hys} @0.0009 Ts^{-1}), and T_B^{100} is found to be 13.9 K. The combination of an apt anisotropy with Tb^{III} is linked with strong exchange coupling *via* the N_2^{3-} bridge. While in the same work, the exchange between the Tb^{III} and the bridging ligand N_2^{3-} has not been reported, the strong exchange has been reported with the Gd analogue {[[$(Me_3Si)_2N]_2$-(THF)Gd}$_2$(μ-η$_2$:η$_2$-N_2)$^-$ (**37-Gd**)[39] of the same complex, which is found to be −27 cm^{-1}. The Dy (**37-Dy**) analogue of the same show T_B^{hys} of 8.3 K (@0.08 T s^{-1}). For complex **37-Gd**, we have performed detailed electronic structure calculations, which unequivocally prove the presence of direct overlap between the Gd(III) 4f orbitals and the radical π* orbital. This direct interaction may give both ferromagnetic and antiferromagnetic contributions to the total exchange. The charge transfer from the radical π* orbitals to the 5d/6s orbital of the Gd(III) ion always leads to ferromagnetic exchange. The nature of the net exchange between the two depends on these competing factors. The strength of the exchange is attributed to the nature of the orbital that possesses the unpaired electron, and if the radical orbital is less delocalised, this often yields strong exchange interaction.[131,132] Further, Chibotaru *et al.* elucidated the reason for the large U_{eff} and T_B values observed and the effect of strength of exchange interaction on magnetization blocking for the complex **37-Tb** using *ab initio* and DFT calculations. For such highly anisotropic complexes, there is a strong intermixing of the entire CF spectrum arising from the ground m_J levels with the $S = \frac{1}{2}$ spin of the radical. The low-lying exchange spectrum for the complex **37-Tb** has been represented in Fig. 14 with the admixed CF states on the Tb sites to the exchange states. The transverse g-factors for the ground exchange KD (QTM depends on the square of this parameter as per eqn (5)–(7)) are found to be in the order of ∼10^{-5} to 10^{-6}, and hence the QTM of the order ∼10^{-6} has been estimated. Such a small and negligible value demonstrates the observation of large coercivity and quenching of QTM at zero-field in the measured hysteresis loop.[88]

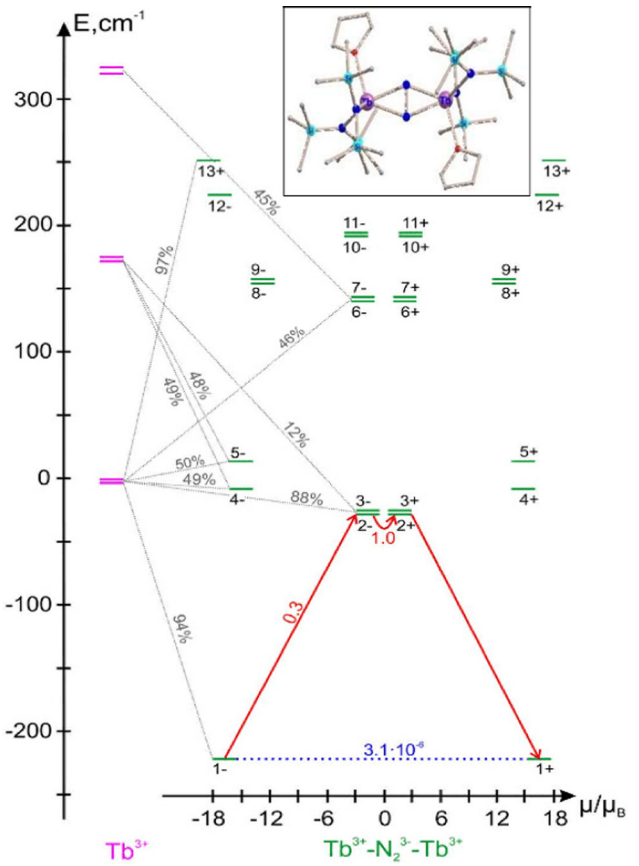

Fig. 14 The low-lying exchange spectrum and the magnetization blocking barrier in $Tb_2N_2^{3-}$ (**37-Tb**) complex. Reproduced from ref. 88 with permission from [Springer Nature], copyright [2016].

The most prolific example with extremely large magnetic exchange coupling reported so far is with the endohedral fullerenes. Our group has successfully predicted the large exchange coupling in the Gd_2@C79N(**38-Gd**) complexes, and their

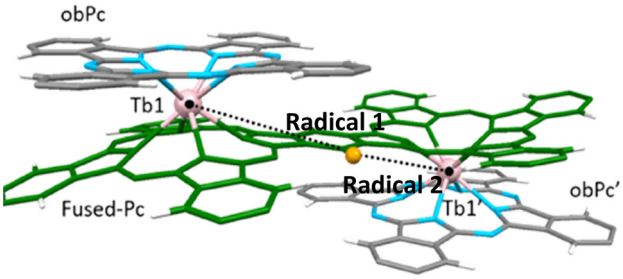

Fig. 15 Structure of the complex [(obPc)Tb(Fused-Pc)Tb(obPc)] (**36**). Reproduced from ref. 124 with permission from [American Chemical Society], copyright [2003].

magnetic properties have been investigated computationally through *ab initio* and density functional calculations.[133] The Gd_2@C79N(**38-Gd**) was found to show a record high exchange coupling between the Gd-rad ($J_{Gd\text{-}radical}$ DFT+378 cm^{-1}), which was later verified experimentally by two groups simultaneously by Gao *et al.*[134] and Popov *et al.* yielding $J_{Gd\text{-}radical}$ value of 350 ± 20 cm^{-1} and 340 ± 20 cm^{-1}, respectively.[135] As expected, replacing the Gd with Dy for the complex Dy_2@C79N (**38-Dy**), a more considerable barrier height up to 582 to 713 cm^{-1} (Fig. 16c) has been predicted and later verified by experiments with U_{eff} = 465 cm^{-1} and T_B^{hys} of 24 K @0.02 T s^{-1} (T_B^{FZ} = 21 K).[136] The Tb analogue [Tb_2@C79N](**38-Tb**) has been reported with an U_{eff} barrier of 526 cm^{-1} where the QTM is quenched, and relaxation follows the Orbach process. The strong exchange facilitates reaching a T_B^{hys} value of 27 K (@0.0029 T s^{-1}) (T_B^{100} = 24 K) for the corresponding complex.[137] These reports emphasise the importance of *ab initio* calculations in accurately predicting the suitability of molecules that could yield SMM characteristics and have boosted the predictive power of such methods.

Popov *et al.* worked on such complexes extensively where lanthanide-encapsulated fullerene was synthesized and coupled *via* radical between the two lanthanides.[138] Particularly they have reported [Dy_2@C80(CH_2Ph)](**39-Dy**)[139] where radical induced in the cage was stabilised. This molecule also yields strong SMM performance with the U_{eff} values of 426 cm^{-1} and T_B^{hys} of 22 K

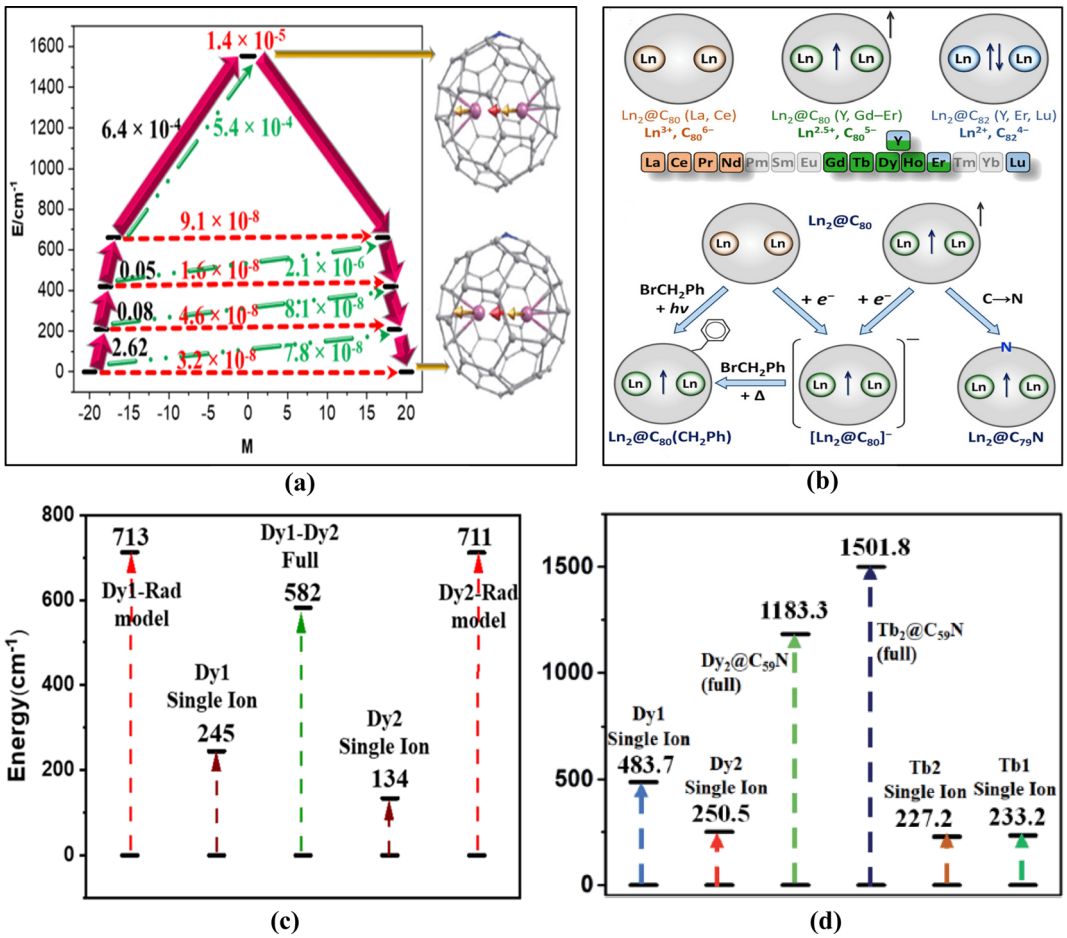

Fig. 16 (a) The POLY_ANISO computed relaxation mechanism of Tb_2@C59N-Cs (**40-Tb**). The anisotropy axis of the metal (represented by yellow) and radical (represented by red) centre are shown on the right. (b) Representation on different Ln–Ln bonding inside fullerene for all 14 lanthanides, (c) diagrammatic representation of the estimated single ion and exchange-coupled U_{cal} for Dy_2@C79N (**38-Dy**), (d) Dy_2@C59N-Cs (**40-Dy**) and Tb_2@C59N-Cs(**40-Tb**). Reproduced from ref. 133, 138 and 141 with permission from [Royal Society of Chemistry], copyright [2015], [American Chemical Society], copyright[2019] and [Royal Society of Chemistry], copyright [2021], respectively.

(@0.0029 T s^{-1}; T_B^{FZ} = 21.9 K and T_B^{100} = 18 K). This has been later extended to other lanthanides Ln_2@C80(CH_2Ph), Ln_2 = Y_2(**39-Y**), Gd_2(**39-Gd**), Tb_2(**39-Tb**), Ho_2(**39-Ho**), Er_2(**39-Er**), TbY(**39-TbY**), and TbGd(**39-TbGd**)).[140] The Tb analogue (**39-Tb**) in this series shows a T_B^{hys} of 28.9 K (@0.0095 T s^{-1}; T_B^{FZ} = 2.9 K and T_B^{100} = 25.2 K, U_{eff} = 555 cm^{-1}), which is one of the highest among all reported dimers.[140] The strong exchange coupling observed in endohedral fullerene **39-Gd** to the peculiar behaviour of the fullerene cage encapsulating the Gd_2 ion leading to Gd_2^{5+} and C_{80}^{5-} fragments with one additional electron found to be delocalised between the Gd···Gd bond that mediates a strong exchange.[138] However, such electron transfer was correlated to the nature of the Ln ions with La-Nd proposed to yield $Ln_2^{6+}\cdots C_{80}^{6-}$ state, Gd–Er yield $Ln_2^{5+}\cdots C_{80}^{5-}$ state, and Lu yield $Ln_2^{4+}\cdots C_{82}^{4-}$ state (Fig. 16b). This model proposed to predict a generation of radicals for Gd to Er ions, which are expected to yield superior SMM characteristics.[138] Our group has explored the Ln encapsulated smaller fullerene (Gd_2@C59N, **40-Gd**) to enhance the J_{exch}, and we have achieved the exchange value as high as +867 cm^{-1} between Gd-radical.[141] For the Dy (**40-Dy**) and Tb (**40-Tb**) analogue, an U_{cal} value of 1183 cm^{-1} and 1502 cm^{-1} have been obtained, respectively, from the exchanged coupled state with relaxation happening from the 4th excited state (Fig. 16a and d). As this predicted value is twice as much reported for the Gd_2@C79N, make them a very attractive target for potential new generation SMMs.

The question that strikes us now is how the exchange could be significantly enhanced further (by orders of magnitude) in classes of complexes other than endohedral fullerenes. Recently three lanthanides have been coupled with a soft donor like *S* with a MoS_4^{3-} bridging motif [$Co(C_5Me_5)_2$][$(C_5Me_5)_2Ln(\mu$-S)$_2$-Mo(μ-S)$_2$Ln(C_5Me_5)$_2$] (Ln = Gd (**41-Gd**), Dy (**41-Dy**) and Tb (**41-Tb**)).[142] The exchange between the Gd-Mo has been reported to be +16 cm^{-1}. A large charge transfer from the singly occupied Mo^V $4d_z^2$ orbital to 5d empty orbitals of the lanthanide is found to be responsible for the large ferromagnetic exchange. Another strategy to increase the exchange interactions would be to increase the number of radicals[123] interacting with a metal centre, *i.e.* instead of one radical if multiple radicals are coupled with Ln ions, this could effectively increase the ground-state-excited-state gap leading to a stronger QTM quenching. This concept has been demonstrated in [$Ln(L^{\bullet -})_3$][L = 2,6-diisopropyl-N-(2-pyridinylmethylene)-phenylamine](Ln = **42-Dy**, **42-Er**, **42-Y**) complex with three radicals bridging to an Ln(III) ion yielding a moderate SMM characteristic even for a nearly ideal octahedral geometry which is expected to yield no anisotropy (Fig. 17a).[143]

An atypical way to improve this exchange is by introducing a lanthanide-transition metal direct bond. The first SMM with such a molecule was reported by Nippe *et al.*, where they introduced a direct bond between the Dy and Fe and Ru having the molecular formula [$PyCp_2DyMCp(CO)_2$] (M = Fe(I) (**43-Dy-Fe**), Ru(I) (**43-Dy-Ru**) and here $PyCp_2$ = 2,6-$(CH_2C_5H_3)_2C_5H_3N]_2^-$].[144] Since Fe and Ru are diamagnetic due to their low-spin state, they do not offer any exchange with the Ln^{III} centre. Recently we have reported a theoretical approach to enhance the direct exchange between the Ln–TM by incorporating the paramagnetic transition metal ion in place of the diamagnetic 3d/4d metals. In such a system, the direct interaction between the Gd–TM ([$PyCp_2$-LnMCp$(CO)_2$], Ln = (**43-Gd**), TM = V (**43-Gd-V**), Mn(**43-Gd-Mn**), Co(**43-Gd-Co**)) (Fig. 17b) has been calculated to be in the range of −40 cm^{-1} to −262 cm^{-1}.[145] Not only the magnitude of exchange but also the nature of exchange can be tuned in such an approach. The CASSCF calculations for the Dy (**43-Dy-M**, M = V, Mn, Co) analogue of the above complexes were predicted to be superior magnets as the QTM is completely quenched for the ground states in the exchanged coupled states, setting the stage for a new generation of SMMs. Another example is [Er^{III}-$(Re^ICp_2)_3$][146] (**44**) (Fig. 18a) molecule with a direct $Er^{III}\cdots Re^I$ metal–metal bond and this molecule exhibited a U_{eff} value of 198 cm^{-1}. This value exceeds the U_{eff} value reported for [$Er(NSiMe_3)_3$](**45**) molecule suggesting a stronger crystal field environment provided by the metal–metal bond compared to ligands such as nitrogen and suggesting Er^{III} as a potential alternative to the dominant Dy^{III} ion in this area.

Similarly, if two lanthanides could be coupled together through a direct bond, the exchange interaction between Ln–Ln can also be enhanced significantly. Very recently, Long *et al.* reported the Ln–Ln supported direct bond in a complex having the molecular formula [$(Cp^iPr_5)_2Ln_2I_3$] (Cp^iPr_5,pentaisopropyl-cyclopentadienyl; Ln is **46-Gd**, **46-Tb**, or **46-Dy**) where the

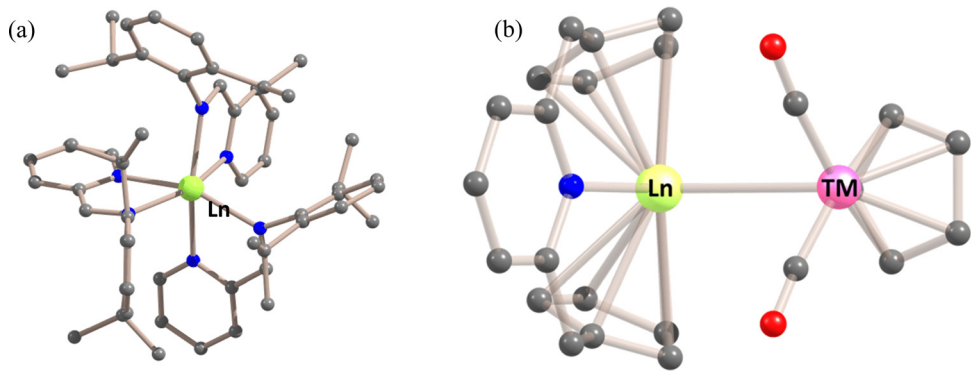

Fig. 17 Crystal structures of the complexes (a) **42-Ln** and (b) **43-Ln.** Reproduced from ref. 143 and 145 with permission from [American Chemical Society], copyright [2018] and [Royal Society of Chemistry], copyright [2021], respectively.

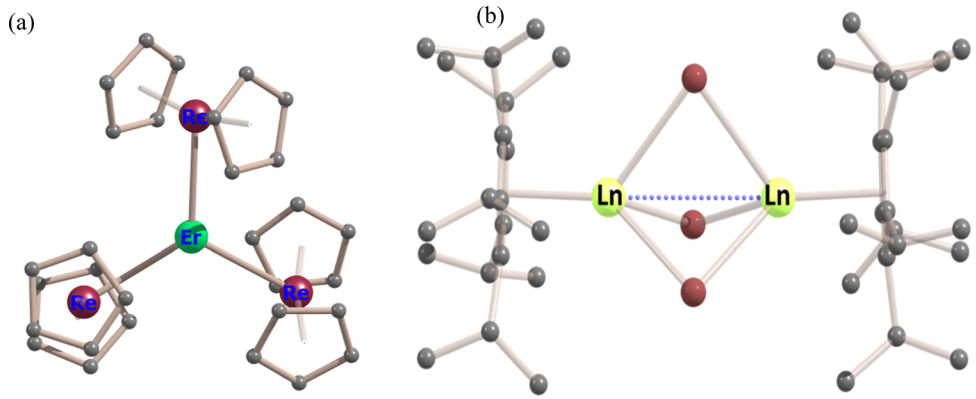

Fig. 18 Crystal structures of the molecule (a) **44** and (b) **41** containing Ln–TM and Ln–Ln metal bonding. Reproduced from ref. 146 and 147 with permission from [Springer Nature], copyright [2022] and [Science], copyright [2022], respectively.

exchange is found to be +389 cm^{-1} which is showing a magnetic coercivity of 14 T at 60 K, proving our hypothesis proposed (Fig. 18b).[147] Another way to enhance this could be to couple the lanthanide in triple-decker or multi-decker complexes in their unusual oxidation states, such as Ln^{II}. Since an extra electron is available for such a system, which may go to 4f, 5d, or 6s orbitals, a larger exchange is expected if the electron moves to these orbitals. The bonding scenario found here is similar to the one studied in endohedral fullerenes, such as **38-Gd** or **39-Gd**.

2.4. Quenching the QTM using external stimuli such as an electric field and pressure

Many non-chemical methods to quench QTM have been gaining attention, including employing external stimuli on a known molecule to modulate the QTM. The external stimuli include pressure and electric field, or the tip of a microscope such as STM to modulate geometries, *etc.* The anisotropy has been successfully modulated through an electric field and has been well established in the case of transition metal SMMs.[148,149] Recently; we have explored the application of electric fields on low coordinate Ln-SIMs using computational methods.[150] An application of an electric field in a particular direction is subjected to the nature of lanthanides and the surrounding environment. For this, three of the well-known SIMs with Dy ($[Dy(Py)_5(O^tBu)_2]^+$(**2**),[58] $[Dy(Cp^{Me3})_2Cl$ or $(Cp^{ttt})_2DyCl]^{151}$(**47**) and Er ($[Er\{N(SiMe_3)_2\}_3.3Cl]^-$(**48**))[152] have been taken into consideration to check the effect of the electric field. For complex **2**, the application of an electric field in the *z*-direction (direction same as that of g_{zz} axis; Fig. 19a and b), a decrease in barrier height from 1118 cm^{-1} (2^{opt}; denote optimised structure of **2** in the presence of electric field) to 1108 cm^{-1} (at the oriented external electric field (OEEF) = 0.2 V $Å^{-1}$) to 1040 cm^{-1} (at OEEF = 0.6 V $Å^{-1}$) has been noticed due to lengthening of one of the Dy–O axial bond and an asymmetric shortening of the other Dy–O bond with the relaxation predict to occur *via* the 4th excited state. The application of an electric field in the equatorial direction (x-direction) further reduces the U_{cal} value to 939 cm^{-1} (OEEF = 0.6 $VÅ^{-1}$) due to Dy–O–Dy angle bending (157°) compared to the optimised geometry (178°). Similarly, for complex **47**, the application of electric field in the *z*-direction, produces a remarkable enhancement in the barrier height from 144 cm^{-1} to 519 cm^{-1} at 1.1 $VÅ^{-1}$ OEEF. For complex **48,** the application of an OEEF along the g_{zz} axis (*i.e.* along the Er–Cl bond) enhanced the value of U_{cal} from 163 cm^{-1} at 0.2 $VÅ^{-1}$ to a remarkable 317 cm^{-1} at 1.3 $VÅ^{-1}$. This estimate is one of the highest obtained for any Er(III) SIMs. Computed transition moment probability for QTM (and TA-QTM) values revealed a smooth decrease of these values from 2.2 μ_B at 0.2 $VÅ^{-1}$ to 1.3 μ_B at 1.3 $VÅ^{-1}$. In addition, a smooth linear increase of the negative $B_0{}^2$ parameter was observed for complex **48** under the applied electric field range along the +*z* direction.[150] Certainly, this approach is a convenient method to induce/increase magnetic properties for a poor-performing single-molecule magnet. The electric field can be a useful tool for increasing the anisotropic barrier and can also be applied to dinuclear or multinuclear systems to manipulate/tune the nature and strength of magnetic exchange interaction between the paramagnetic metal centres. As the nature and strength of magnetic exchange strongly depend on the structural parameters, *i.e.* the bond distance and bond angles,[90,132,153] and the application of external electric field can be used to fine-tune these structural parameters, which in turn alters the exchange interaction. Thus one can use this approach to alter the sign and strength of *J* values and hence the QTM effects. This has been demonstrated experimentally by several groups where the application of an electric field was found to alter the *J* values.[154–157]

Other external stimuli that can be utilized to tune the anisotropy of the metal ion are external pressure.[158,159] By applying an external pressure in a particular crystal, the direction of the g_{zz} axis can be controlled and hence the magnetic relaxation processes.[158,160] However, the external pressure applied depends on the nature of the structure, geometry, presence of solvate/counter ions *etc.* The presence of first excited energy levels with significantly different orientations of its anisotropy tensor; sufficiently low energies of such levels so that they can mix with the ground state; and the possibility of tuning their energies by small geometrical perturbations.[161,162] This has been studied recently by Totti *et al.* in the molecule $\{Na[DyDOTA(H_2O)]\cdot 4H_2O\}$ (**49**) (H_4DOTA = 1,4,7,10 tetraazacyclododecane-1,4,7,10-*N*,*N*′,*N*″,*N*‴-tetraacetic acid), where the possibility of alternation of anisotropic

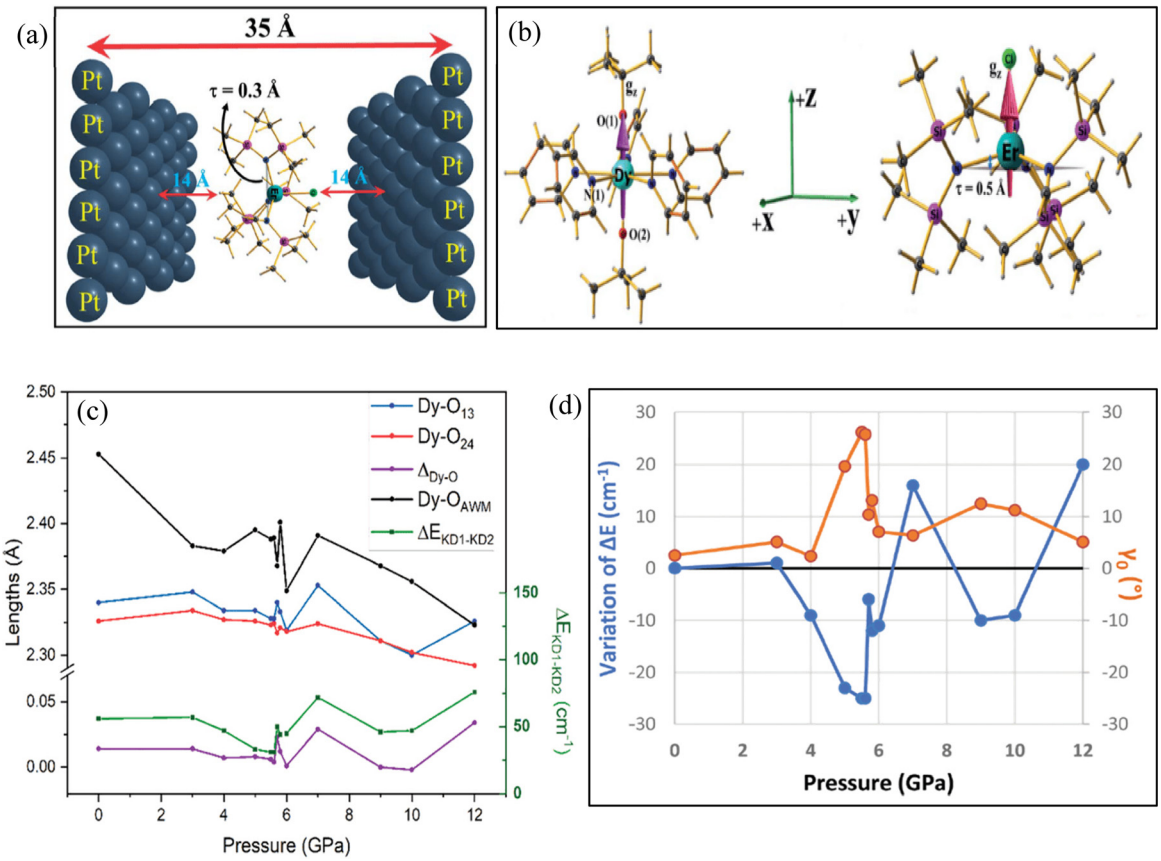

Fig. 19 Arrangement of the application of an external electric field, (a) arrangement of applying an external electric field by placing point charges on two opposite Pt (111) layers, (b) orientation of the molecules along a different axis, (c) variation of various structural parameters by applying external pressure, (d) variation of the energy gap between the ground and first excited KDs with respect to the value computed at 0 G Pa (blue) and the angle between the computed and experimental magnetic easy axis (orange). Reproduced from ref. 150 and 163 with permission from [Royal Society of Chemistry], copyright [2020] and [Royal Society of Chemistry], copyright [2021], respectively.

direction by inducing pressure has been shown.[163] Since the anisotropy of a metal ion is strongly structurally dependent, by applying pressure, the volume of the crystal structure shrinks, resulting in a change in various structural parameters and hence the anisotropy. Depending on the amount of applied pressure, if the Dy–O (a particular) bond shrinks (expands), the ground state KDs stabilizes (destabilizes) compared to normal geometry. The variation of ground to 1st excited state energy gap by external pressure is represented in Fig. 13c and d. Contrary to the application of pressure, tuning the anisotropy by employing an electric field seems a better approach, as, for the latter, the required condition for an SMM to have pronounced anisotropy is less compared to the pressure studies. In terms of practicality, applying pressure is easier than modulating the electric field, which is still an area at its nascent stage.

2.5. Avoiding the QTM by stabilizing toroidal state as the ground state in 4f and {3d–4f} Complexes

Apart from the conventional polarization and magnetization electromagnetic moment, the vortex distribution of magnetic dipoles can lead to the third kind of electromagnetic moment, the toroidal moment.[164] The molecules for which the bistability can be achieved due to the toroidal states are known as Single Molecule Toroic (SMTs)[165] and are potential alternatives to SMMs for futuristic applications in quantum computing and information storage devices. Such molecules can be regarded as multi-spin systems breaking both space inversion and time reversal symmetries, which can be achieved by persistent orbital currents or certain spin orderings. The mathematical expression for the toroidal moment (t) will take the form $t\alpha\sum_i r_i \times S_i$, where r_i = displacement from the centre of the ring and S_i = spin of the systems forming ring topology (Fig. 20a).[166,167] The multi-spin system requires a toroidal arrangement of the individual magnetic moments in a plane to show toroic behaviour. The most promising approach to constructing a toroidal moment is building wheel-shaped complexes with high intramolecular symmetry and strong intramolecular dipolar interactions employing strongly anisotropic metal ions.

Toroidal magnetic moment can be a potential alternative to avoid QTM of the m_J states. Since the toroidal moment arises due to spin vertex distribution in a clockwise or anticlockwise manner if the toroidal states are stabilized as the ground state, the QTM can be avoided (Fig. 20).[167,168] The Dy_3 ([$Dy_3(\mu_3$-

$OH)_2L_3Cl(H_2O)_5]C_{l5}\cdot 19H_2O$, L= *o*-vanillin)(**50**), triangle reported by Powell *et al.* with the *o*-vanillin ligand is the first of this kind where the non-magnetic ground state has been achieved, which was later confirmed to be due to the toroidal moment.[169,170] Later several other examples with $[Dy_4(\mu_3\text{-}OH)_2(\mu\text{-}OH)_2(2,2\text{-bpt})_4(NO_3)_4(EtOH)_2]$[171] (where [1; 2,2-bptH = 3,5-bis(pyridin-2-yl)-1,2,4-triazole]) **51**), $Dy_6([Dy(Htea)(NO_3)]_6\cdot 8MeOH$ (H_3tea = triethanolamine)**52-Dy**),[172] Cu_3Dy_3 ($\{[Cu(L)_2CH_3OH][L_3Ln_3(\mu_3\text{-}OH)_2(NO_3)_4]\}_n$,L = *o*-vanillin) (**53**),[173] Ln_6Cu_6, Ln= Tb and $Dy([Ln_6Cu_6(H_2L)_6Cl_{12}(H_2O)_6]5ClO_4\cdot OH\cdot xH_2O)$ (**54-Tb**, **54-Dy**),[174] Dy_4 cubane Dy_4 ($[Dy_4(Bppd)_4(\mu_3\text{-}OH)_4(Pa)_4(H_2O)_4]\cdot 0.333H_2O$ (where BppdH = 1,3-bis(pyridin-4-yl)propane-1,3-dione and PaH = 2-Picolinic acid) **55**)[175] core was reported, which is found to be showing the toroidal moment. Along with this, the investigation of the toroidal moment in Tb_4 ($[Tb_4(LH_2)_2(O_3P^{t}\text{-}Bu)_2(\mu_2\text{-}\eta^1\eta^1tfa)_2][2Cl]$, LH_2 is a Schiff base ligand, **56**) systems has been studied by us earlier. Very recently, Tang *et al.* also reported a Tb_4 SMT molecule with Schiff's base ligand having the molecular formula $[Tb_4(\mu_4\text{-}OH)(HL_2)_4(NCS)_2]\cdot NCS\cdot CH_3CN\cdot 5CH_3OH$ (**57**).[176] The Dy_6 toroidal systems have been extended to other Ln-systems other than Dy^{III} ($[Ln^{III}_6(teaH)_6(NO_3)_6]\cdot 8MeOH$, Ln = **52-Tb**, **52-Ho**, **52-Er**) by us with the report of the Ln_6 series complex.[177] It is clear from the above examples that, to have toroidal magnetic states, a molecule should possess (i) circular molecular symmetry (triangles, squares, and hexagons are the best candidates), (ii) local magnetic moment (strong anisotropy), and (iii) strong intra-molecular dipolar interactions.[178] Coupling to Dy_3 *via* a transition metal leads to the ferro and anti-ferrotoroidal states (Fig. 21), which we have reported for the first time in the $CrDy_6$ ($[CrDy_6(OH)_8(ortho\text{-}tol)_{12}(NO_3)(MeOH)_5]\cdot 3MeOH$, (**58-Dy**) systems.[179] The change of Dy^{III} to other oblate ions like Tb^{III} (**58-Tb**) and Ho^{III}(**58-Ho**) in the same $CrDy_6$ core also indicates the presence of FT-AFT states, whereas switching to prolate ions like Er^{III} (**58-Er**) destroys the toroidal properties (Fig. 20d).[180] Hence the role of lanthanide ion and structural topology is very important in determining the toroidal and ferro-toroidal states. Later, such systems have been extensively studied by us with the replacement of connecting transition metal Cr^{III} with diamagnetic ions such as Al^{III} and Co^{III} ($[AlDy_6(OH)_8(ortho\text{-}tol)_{12}(NO_3)(MeOH)_5]\cdot 3MeOH$, **58-Dy-Al**, **58-Dy-Co**) as well as with paramagnetic ions such Fe ($[FeDy_6(OH)_8(ortho\text{-}tol)_{12}(NO_3)(MeOH)_5]\cdot 3MeOH$; **58-Dy-Fe**), and Mn ($[CrDy_6(OH)_8(ortho\text{-}tol)_{12}(NO_3)(MeOH)_5]\cdot 3MeOH$; **58-Dy-Mn**) with NO_3^- and Cl^- counter anions.[181] All these systems are suitable candidates to display either ferro-toroidal or antiferro-toroidal ground state. The dipolar coupling between

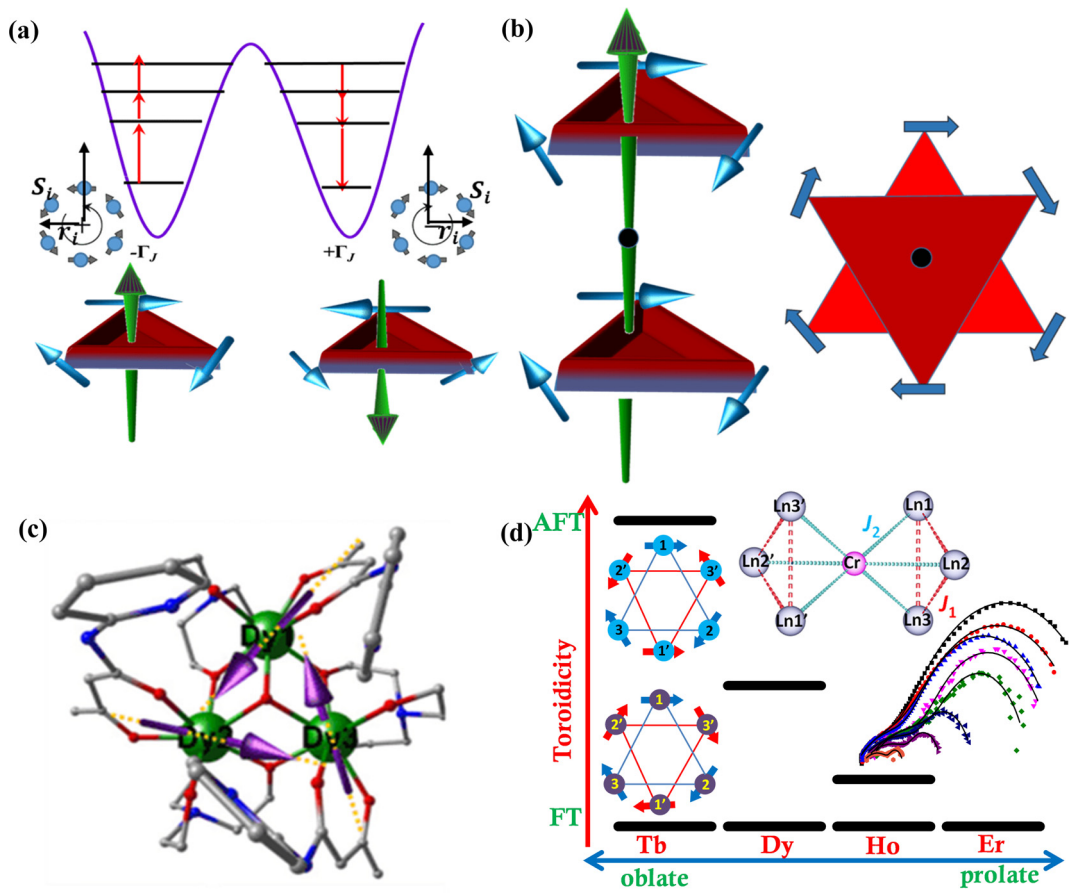

Fig. 20 Schematic representation of (a) toroidal states mimicking SMM behaviour, (b) coupling of two triangles to obtain ferro-toroidal arrangements, (c) Dy_3 showing toroidal behaviour, (d) ferrotoroidal trend in $CrLn_6$ (Ln = Dy, Tb, Ho, Er) complexes. Reproduced from ref. 178 and 180 with permission from [American Chemical Society], copyright [2021] and [John Wiley and Sons], copyright [2018], respectively.

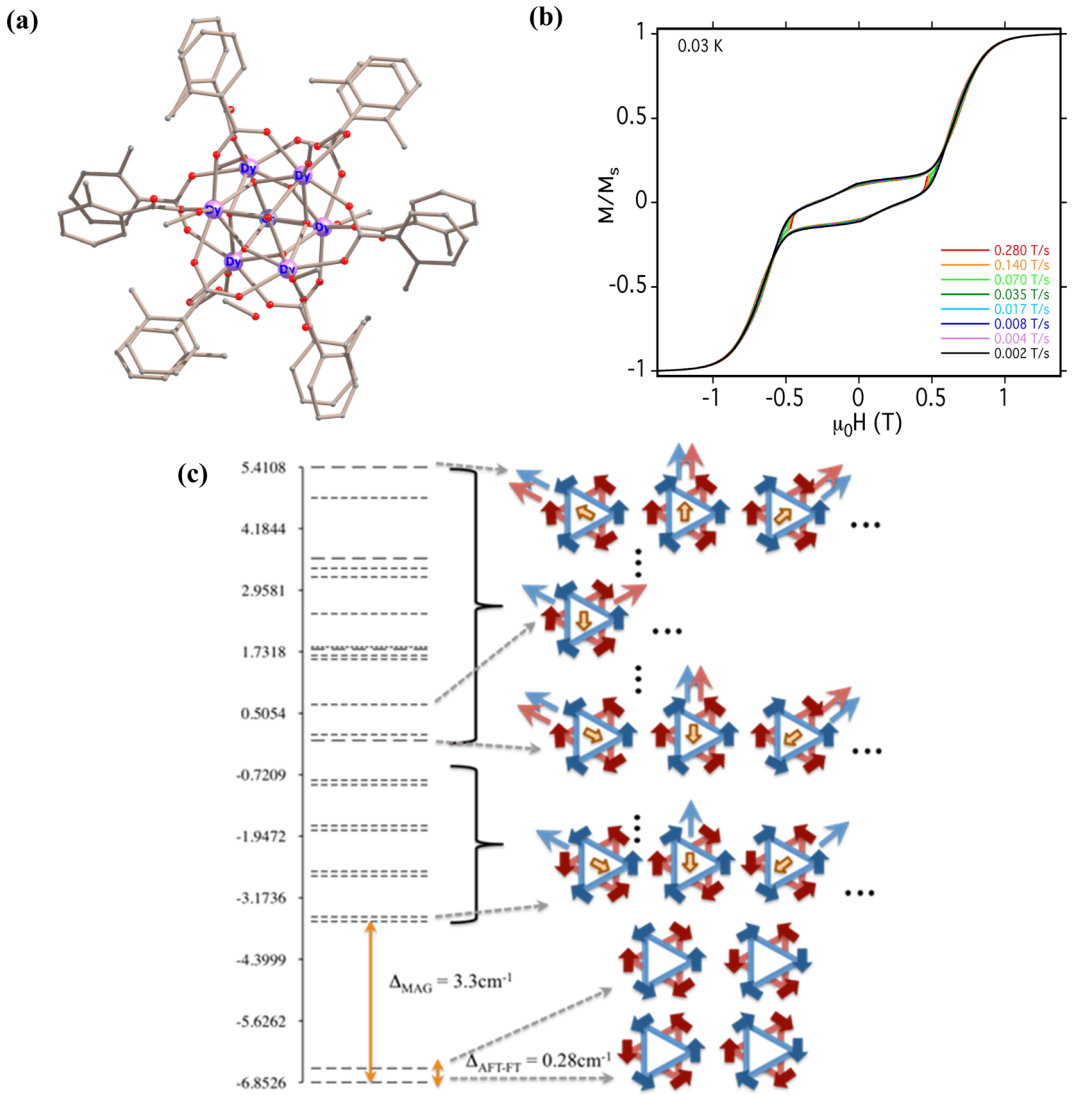

Fig. 21 (a) Crystal structure of complex $CrDy_6$ **(58-Dy)**, (b) single-crystal magnetization (M) *vs.* applied field measurements (μ-SQUID) for the same complex with different field sweep rates at 0.03 K. (c) Energy spectrum of $CrDy_6$ calculated for the low lying doublet. Reproduced from ref. 179 with permission from [Springer Nature], copyright [2017].

the Ln^{III}–Ln^{III} plays the most dominating role in determining the FT-AFT gaps. We have also investigated several other Ln_3 triangle toroidal properties.[178] Various structural topologies connected to the $\{Ln_n\}$ core with circular arrangements have been discovered to produce SMT features. Peripheral ligands were discovered to be critical in controlling the direction of the g_{zz} axis, which was found to be significantly linked with the presence and absence of toroidal moments in such systems. In future, such systems could be a potential alternative for the conventional SMM as the QTM phenomena can be omitted for this class of complexes at their ground state. However, the main challenge here is to obtain isolated toroidal states with the other spin-coupled state strongly destabilised to avoid relaxation *via* these excited states. This seems very challenging as exchange coupling in these clusters is often small, and toroidal state stabilisation arising from the dipolar coupling of the Ln^{III} ions is often weak. An effort to induce an Ln···Ln direct bond and toroidal state could be a strategy that could be achieved in endohedral fullerenes or *via* unconventional organometallic lanthanide complexes in the future.

3. Conclusions

Quenching the Quantum Tunneling of Magnetization (QTM) without an applied magnetic field is one of the prime requirements to enhance the blocking temperature (T_B) for Single-Molecule Magnets (SMMs). In this feature article, we have explored various possibilities to diminish the QTM at zero-field, emphasising the role of DFT and *ab initio* calculations that were instrumental in developing the mechanism of magnetic relaxation. Among various strategies discussed for SIMs,

the importance of local symmetry and the nature of the coordinating atoms were highlighted to quell the QTM effects. Several pseudo-symmetric point groups, such as D_{5h}, D_{6h} *etc.*, were successful SIMs due to suppression of ground state QTM exemplified by the nature of the ligand field and the pseudo local symmetry of the Ln^{III} ions.

Further, a suitable isotopic enrichment can also be an alternative for reducing the QTM as this suppresses the hyperfine coupling, which is often the culprit for the zero-field tunnelling of Kramers doublets. Followed by SIMs, we have discussed how the exchange coupling leads to the quenching of the QTM phenomena in multinuclear SMMs. In this section, we have elaborated on the examples of 3d–4f complexes (super-exchange), radical bridged lanthanide complexes, and endohedral fullerenes (direct exchange) to demonstrate the role of magnetic coupling in quelling the QTM effects. Two different classes of compounds were discussed here, one following a typical super-exchange mechanism, often yielding comparatively smaller exchange interaction and another where a metal–metal/radical bond as a tool to boost the magnetic coupling. Both compounds noted significant ground state tunnelling suppression with stronger exchange coupling, often yielding larger barrier heights or T_B values. This is followed by an approach to tuning the properties by non-chemical methods by employing external pressure or an electric field. Particularly application of an electric field in a certain direction was found to suppress the transverse anisotropy and hence the QTM effect in Ln^{III} SIMs. In the last section, we discussed another emerging class of compounds, namely single-molecule toroics. In this class of compounds, stabilization of non-magnetic toroidal states completely avoids the conventional QTM discussed and shows a significant opening of the hysteresis at zero fields. The challenge of obtaining isolated toroidal states in this class of compounds is elusive.

Conflicts of interest

There are no conflicts to declare.

Acknowledgements

We thank SERB (SB/SJF/2019-20/12; CRG/2022/001697) for funding. AS thanks IITB for the IPDF fellowship. TS thanks CSIR for the fellowship.

References

1 G. Christou, D. Gatteschi, D. N. Hendrickson and R. Sessoli, *MRS Bull.*, 2000, **25**, 66–71.
2 D. Gatteschi, R. Sessoli and J. Villain, *Molecular nanomagnets*, Oxford University Press on Demand, 2006.
3 L. Bogani and W. Wernsdorfer, *Nat. Mater.*, 2008, **7**, 179–186.
4 A. Gaita-Ariño, F. Luis, S. Hill and E. Coronado, *Nat. Chem.*, 2019, **11**, 301–309.
5 E. Coronado, *Nat. Rev. Mater.*, 2020, **5**, 87–104.
6 D. York, *Earth Planet. Sci. Lett.*, 1978, **39**, 94–97.
7 A. Chiesa, F. Cugini, R. Hussain, E. Macaluso, G. Allodi, E. Garlatti, M. Giansiracusa, C. Goodwin, F. Ortu and D. Reta, *Phys. Rev. B: Condens. Matter Mater. Phys.*, 2020, **101**, 174402.
8 A. Zabala-Lekuona, J. M. Seco and E. Colacio, *Coord. Chem. Rev.*, 2021, **441**, 213984.
9 D. N. Woodruff, R. E. Winpenny and R. A. Layfield, *Chem. Rev.*, 2013, **113**, 5110–5148.
10 F.-S. Guo, B. M. Day, Y.-C. Chen, M.-L. Tong, A. Mansikkamäki and R. A. Layfield, *Science*, 2018, **362**, 1400–1403.
11 K. Diller, A. Singha, M. Pivetta, C. Wäckerlin, R. Hellwig, A. Verdini, A. Cossaro, L. Floreano, E. Vélez-Fort and J. Dreiser, *RSC Adv.*, 2019, **9**, 34421–34429.
12 M. Mannini, F. Bertani, C. Tudisco, L. Malavolti, L. Poggini, K. Misztal, D. Menozzi, A. Motta, E. Otero and P. Ohresser, *Nat. Commun.*, 2014, **5**, 4582.
13 A. Cornia and M. Mannini, in *Molecular nanomagnets and related phenomena*, ed. S. Gao, Springer, Berlin Heidelberg, 2014, pp. 293–330.
14 R. Sessoli, D. Gatteschi, A. Caneschi and M. Novak, *Nature*, 1993, **365**, 141–143.
15 G. Aromí and E. K. Brechin, *Single-molecule magnets and related phenomena*, ed. R. Winpenny, Springer, Heidelberg, Germany, 2006, pp. 1–67.
16 J. Larionova, M. Gross, M. Pilkington, H. Andres, H. Stoeckli-Evans, H. U. Güdel and S. Decurtins, *Angew. Chem., Int. Ed.*, 2000, **39**, 1605–1609.
17 M. Affronte, J. Lasjaunias, W. Wernsdorfer, R. Sessoli, D. Gatteschi, S. Heath, A. Fort and A. Rettori, *Phys. Rev. B: Condens. Matter Mater. Phys.*, 2002, **66**, 064408.
18 M. Murugesu, M. Habrych, W. Wernsdorfer, K. A. Abboud and G. Christou, *J. Am. Chem. Soc.*, 2004, **126**, 4766–4767.
19 A. M. Ako, I. J. Hewitt, V. Mereacre, R. Clérac, W. Wernsdorfer, C. E. Anson and A. K. Powell, *Angew. Chem.*, 2006, **118**, 5048–5051.
20 A. J. Tasiopoulos, A. Vinslava, W. Wernsdorfer, K. A. Abboud and G. Christou, *Angew. Chem.*, 2004, **116**, 2169–2173.
21 F. Neese and D. A. Pantazis, *Faraday Discuss.*, 2011, **148**, 229–238.
22 M. Feng and M. L. Tong, *Chem. – Eur. J.*, 2018, **24**, 7574–7594.
23 G. A. Craig and M. Murrie, *Chem. Soc. Rev.*, 2015, **44**, 2135–2147.
24 J. M. Frost, K. L. Harriman and M. Murugesu, *Chem. Sci.*, 2016, **7**, 2470–2491.
25 N. Ishikawa, M. Sugita, T. Ishikawa, S.-Y. Koshihara and Y. Kaizu, *J. Am. Chem. Soc.*, 2003, **125**, 8694–8695.
26 J. Tang and P. Zhang, *Lanthanide single molecule magnets*, Springer, 2015.
27 J. D. Rinehart and J. R. Long, *Chem. Sci.*, 2011, **2**, 2078–2085.
28 J.-L. Liu, Y.-C. Chen and M.-L. Tong, *Chem. Soc. Rev.*, 2018, **47**, 2431–2453.
29 P. Zhang, Y.-N. Guo and J. Tang, *Coord. Chem. Rev.*, 2013, **257**, 1728–1763.
30 D. Shao and X. Y. Wang, *Chin. J. Chem.*, 2020, **38**, 1005–1018.
31 Z. Zhu and J. Tang, *Natl. Sci. Rev.*, 2022, nwac194.
32 A. Dey, P. Kalita and V. Chandrasekhar, *ACS Omega*, 2018, **3**, 9462–9475.
33 S.-D. Jiang and S.-X. Qin, *Inorg. Chem. Front.*, 2015, **2**, 613–619.
34 Y.-C. Chen and M.-L. Tong, *Chem. Sci.*, 2022, **13**, 8716–8726.
35 R. J. Blagg, L. Ungur, F. Tuna, J. Speak, P. Comar, D. Collison, W. Wernsdorfer, E. J. McInnes, L. F. Chibotaru and R. E. Winpenny, *Nat. Chem.*, 2013, **5**, 673–678.
36 J. Villain, F. Hartman-Boutron, R. Sessoli and A. Rettori, *Europhys. Lett.*, 1994, **27**, 159.
37 L. Gu and R. Wu, *Phys. Rev. Lett.*, 2020, **125**, 117203.
38 D. Gatteschi and R. Sessoli, *Angew. Chem., Int. Ed.*, 2003, **42**, 268–297.
39 J. D. Rinehart, M. Fang, W. J. Evans and J. R. Long, *Nat. Chem.*, 2011, **3**, 538–542.
40 S. Miyashita, *J. Phys. Soc. Jpn.*, 1995, **64**, 3207–3214.
41 G. Rose and P. Stamp, *J. Low Temp. Phys.*, 1998, **113**, 1153–1158.
42 M. N. Leuenberger and D. Loss, *Phys. Rev. B: Condens. Matter Mater. Phys.*, 2000, **61**, 12200.
43 M. Thorwart, M. Grifoni and P. Hänggi, *Phys. Rev. Lett.*, 2000, **85**, 860.
44 S. M. Aubin, N. R. Dilley, L. Pardi, J. Krzystek, M. W. Wemple, L.-C. Brunel, M. B. Maple, G. Christou and D. N. Hendrickson, *J. Am. Chem. Soc.*, 1998, **120**, 4991–5004.
45 E. K. Brechin, C. Boskovic, W. Wernsdorfer, J. Yoo, A. Yamaguchi, E. C. Sanudo, T. R. Concolino, A. L. Rheingold, H. Ishimoto and D. N. Hendrickson, *J. Am. Chem. Soc.*, 2002, **124**, 9710–9711.

46 L. Lecren, W. Wernsdorfer, Y.-G. Li, O. Roubeau, H. Miyasaka and R. Clérac, *J. Am. Chem. Soc.*, 2005, **127**, 11311–11317.
47 L. Ungur, M. Thewissen, J.-P. Costes, W. Wernsdorfer and L. F. Chibotaru, *Inorg. Chem.*, 2013, **52**, 6328–6337.
48 V. Dohm and P. Fulde, *Z. Phys. B: Condens. Matter*, 1975, **21**, 369–379.
49 N. F. Chilton, D. Collison, E. J. McInnes, R. E. Winpenny and A. Soncini, *Nat. Commun.*, 2013, **4**, 2551.
50 S. K. Singh, T. Gupta and G. Rajaraman, *Inorg. Chem.*, 2014, **53**, 10835–10845.
51 L. Ungur and L. F. Chibotaru, *Phys. Chem. Chem. Phys.*, 2011, **13**, 20086–20090.
52 C. Rudowicz, *J. Phys. Chem. C*, 1985, **18**, 1415.
53 U. Walter, *J. Phys. Chem. Solids*, 1984, **45**, 401–408.
54 L. Ungur, J. J. Le Roy, I. Korobkov, M. Murugesu and L. F. Chibotaru, *Angew. Chem.*, 2014, **126**, 4502–4506.
55 L. F. Chibotaru and L. Ungur, *J. Chem. Phys.*, 2012, **137**, 064112.
56 A. Swain, A. Sarkar and G. Rajaraman, *Chem. – Asian J.*, 2019, **14**, 4056–4073.
57 X. L. Ding, Y. Q. Zhai, T. Han, W. P. Chen, Y. S. Ding and Y. Z. Zheng, *Chem. – Eur. J.*, 2021, **27**, 2623–2627.
58 Y. S. Ding, N. F. Chilton, R. E. Winpenny and Y. Z. Zheng, *Angew. Chem., Int. Ed.*, 2016, **55**, 16071–16074.
59 A. B. Canaj, S. Dey, E. R. Martí, C. Wilson, G. Rajaraman and M. Murrie, *Angew. Chem., Int. Ed.*, 2019, **58**, 14146–14151.
60 A. Lunghi and S. Sanvito, *J. Chem. Phys.*, 2020, **153**, 174113.
61 A. Lunghi, F. Totti, R. Sessoli and S. Sanvito, *Nat. Commun.*, 2017, **8**, 14620.
62 L. Scherthan, R. F. Pfleger, H. Auerbach, T. Hochdörffer, J. A. Wolny, W. Bi, J. Zhao, M. Y. Hu, E. E. Alp and C. E. Anson, *Angew. Chem., Int. Ed.*, 2020, **59**, 8818–8822.
63 A. Lunghi, F. Totti, S. Sanvito and R. Sessoli, *Chem. Sci.*, 2017, **8**, 6051–6059.
64 S. K. Gupta, T. Rajeshkumar, G. Rajaraman and R. Murugavel, *Chem. Sci.*, 2016, **7**, 5181–5191.
65 S. K. Gupta, T. Rajeshkumar, G. Rajaraman and R. Murugavel, *Dalton Trans.*, 2018, **47**, 357–366.
66 M. A. Sørensen, U. B. Hansen, M. Perfetti, K. S. Pedersen, E. Bartolomé, G. G. Simeoni, H. Mutka, S. Rols, M. Jeong, I. Zivkovic, M. Retuerto, A. Arauzo, J. Bartolomé, S. Piligkos, H. Weihe, L. H. Doerrer, J. van Slageren, H. M. Rønnow, K. Lefmann and J. Bendix, *Nat. Commun.*, 2018, **9**, 1292.
67 R. Pederson, A. L. Wysocki, N. Mayhall and K. Park, *J. Phys. Chem. A*, 2019, **123**, 6996–7006.
68 P. Zhang, L. Zhang, C. Wang, S. Xue, S.-Y. Lin and J. Tang, *J. Am. Chem. Soc.*, 2014, **136**, 4484–4487.
69 S. K. Singh, T. Gupta, M. Shanmugam and G. Rajaraman, *Chem. Commun.*, 2014, **50**, 15513–15516.
70 S. K. Singh, B. Pandey, G. Velmurugan and G. Rajaraman, *Dalton Trans.*, 2017, **46**, 11913–11924.
71 C. A. Goodwin, F. Ortu, D. Reta, N. F. Chilton and D. P. Mills, *Nature*, 2017, **548**, 439–442.
72 K. R. McClain, C. A. Gould, K. Chakarawet, S. J. Teat, T. J. Groshens, J. R. Long and B. G. Harvey, *Chem. Sci.*, 2018, **9**, 8492–8503.
73 C. A. Gould, K. R. McClain, J. M. Yu, T. J. Groshens, F. Furche, B. G. Harvey and J. R. Long, *J. Am. Chem. Soc.*, 2019, **141**, 12967–12973.
74 K. R. Meihaus and J. R. Long, *J. Am. Chem. Soc.*, 2013, **135**, 17952–17957.
75 J. J. Le Roy, L. Ungur, I. Korobkov, L. F. Chibotaru and M. Murugesu, *J. Am. Chem. Soc.*, 2014, **136**, 8003–8010.
76 T. Sharma, M. K. Singh, R. Gupta, M. Khatua and G. Rajaraman, *Chem. Sci.*, 2021, **12**, 11506–11514.
77 A. Abragam and B. Bleaney, *Electron paramagnetic resonance of transition ions*, Oxford University Press, 2012.
78 F. Pointillart, K. Bernot, S. Golhen, B. Le Guennic, T. Guizouarn, L. Ouahab and O. Cador, *Angew. Chem., Int. Ed.*, 2015, **127**, 1524–1527.
79 Y. Kishi, F. Pointillart, B. Lefeuvre, F. Riobé, B. Le Guennic, S. Golhen, O. Cador, O. Maury, H. Fujiwara and L. Ouahab, *Chem. Commun.*, 2017, **53**, 3575–3578.
80 T. T. Da Cunha, J. Jung, M.-E. Boulon, G. Campo, F. Pointillart, C. L. Pereira, B. Le Guennic, O. Cador, K. Bernot and F. Pineider, *J. Am. Chem. Soc.*, 2013, **135**, 16332–16335.
81 J. Flores Gonzalez, H. Douib, B. Le Guennic, F. Pointillart and O. Cador, *Inorg. Chem.*, 2021, **60**, 540–544.
82 W. Zhang, A. Muhtadi, N. Iwahara, L. Ungur and L. F. Chibotaru, *Angew. Chem., Int. Ed.*, 2020, **59**, 12720–12724.
83 R. L. Smith, A. L. Wysocki and K. Park, *Phys. Chem. Chem. Phys.*, 2020, **22**, 21793–21800.
84 V. Dubrovin, A. A. Popov and S. Avdoshenko, *Chem. Commun.*, 2019, **55**, 13963–13966.
85 R. Tiron, W. Wernsdorfer, N. Aliaga-Alcalde and G. Christou, *Phys. Rev. B: Condens. Matter Mater. Phys.*, 2003, **68**, 140407.
86 L. Zhao, J. Wu, H. Ke and J. Tang, *Inorg. Chem.*, 2014, **53**, 3519–3525.
87 K. R. Vignesh, S. K. Langley, K. S. Murray and G. Rajaraman, *Chem. – Eur. J.*, 2017, **23**, 1654–1666.
88 V. Vieru, N. Iwahara, L. Ungur and L. F. Chibotaru, *Sci. Rep.*, 2016, **6**, 24046.
89 T. Gupta, M. F. Beg and G. Rajaraman, *Inorg. Chem.*, 2016, **55**, 11201–11215.
90 G. Rajaraman, F. Totti, A. Bencini, A. Caneschi, R. Sessoli and D. Gatteschi, *Dalton Trans.*, 2009, 3153–3161.
91 Y.-N. Guo, G.-F. Xu, W. Wernsdorfer, L. Ungur, Y. Guo, J. Tang, H.-J. Zhang, L. F. Chibotaru and A. K. Powell, *J. Am. Chem. Soc.*, 2011, **133**, 11948–11951.
92 W. Zhang, S.-M. Xu, Z.-X. Zhu, J. Ru, Y.-Q. Zhang and M.-X. Yao, *New J. Chem.*, 2020, **44**, 2083–2090.
93 K. Bernot, C. Daiguebonne, G. Calvez, Y. Suffren and O. Guillou, *Acc. Chem. Res.*, 2021, **54**, 427–440.
94 Z. Zheng and P. C. Burns, *Recent development in clusters of rare earths and actinides: chemistry and materials*, Springer, 2017.
95 I. F. Díaz-Ortega, J. M. Herrera, Á. Reyes Carmona, J. R. Galán-Mascarós, S. Dey, H. Nojiri, G. Rajaraman and E. Colacio, *Front. Chem.*, 2018, 537.
96 N. Lalioti, V. Nastopoulos, N. Panagiotou, A. Tasiopoulos, N. Ioannidis, J. van Slageren, P. Zhang, G. Rajaraman, A. Swain and V. Tangoulis, *Dalton Trans.*, 2022, **51**, 1985–1994.
97 S. Ghosh, S. Mandal, M. K. Singh, C.-M. Liu, G. Rajaraman and S. Mohanta, *Dalton Trans.*, 2018, **47**, 11455–11469.
98 I. F. Diaz-Ortega, J. M. Herrera, D. Aravena, E. Ruiz, T. Gupta, G. Rajaraman, H. Nojiri and E. Colacio, *Inorg. Chem.*, 2018, **57**, 6362–6375.
99 P. Kumar, A. Swain, J. Acharya, Y. Li, V. Kumar, G. Rajaraman, E. Colacio and V. Chandrasekhar, *Inorg. Chem.*, 2022, **61**, 11600–11621.
100 P. Kumar, S. Biswas, A. Swain, J. Acharya, V. Kumar, P. Kalita, J. F. Gonzalez, O. Cador, F. Pointillart and G. Rajaraman, *Inorg. Chem.*, 2021, **60**, 8530–8545.
101 S. Dey and G. Rajaraman, *Dalton Trans.*, 2020, **49**, 14781–14785.
102 G. Velkos, W. Yang, Y.-R. Yao, S. M. Sudarkova, F. Liu, S. M. Avdoshenko, N. Chen and A. A. Popov, *Chem. Commun.*, 2022, **58**, 7164–7167.
103 T. Han, Y.-S. Ding and Y.-Z. Zheng, *Recent development in clusters of rare earths and actinides: chemistry and materials*, Springer, 2016, pp. 209–314.
104 S. Maity, A. Mondal, S. Konar and A. Ghosh, *Dalton Trans.*, 2019, **48**, 15170–15183.
105 J. Li, R.-M. Wei, T.-C. Pu, F. Cao, L. Yang, Y. Han, Y.-Q. Zhang, J.-L. Zuo and Y. Song, *Inorg. Chem. Front.*, 2017, **4**, 114–122.
106 L. R. Piquer and E. C. Sañudo, *Dalton Trans.*, 2015, **44**, 8771–8780.
107 A. Dey, J. Acharya and V. Chandrasekhar, *Chem. – Asian J.*, 2019, **14**, 4433–4453.
108 C. Benelli and D. Gatteschi, *Chem. Rev.*, 2002, **102**, 2369–2388.
109 H.-S. Wang, K. Zhang, Y. Song and Z.-Q. Pan, *Inorg. Chim. Acta*, 2021, **521**, 120318.
110 Y. Peng and A. K. Powell, *Coord. Chem. Rev.*, 2021, **426**, 213490.
111 S. K. Langley, N. F. Chilton, L. Ungur, B. Moubaraki, L. F. Chibotaru and K. S. Murray, *Inorg. Chem.*, 2012, **51**, 11873–11881.
112 S. K. Langley, C. Le, L. Ungur, B. Moubaraki, B. F. Abrahams, L. F. Chibotaru and K. S. Murray, *Inorg. Chem.*, 2015, **54**, 3631–3642.
113 S. K. Langley, D. P. Wielechowski, B. Moubaraki and K. S. Murray, *Chem. Commun.*, 2016, **52**, 10976–10979.
114 S. K. Langley, D. P. Wielechowski, V. Vieru, N. F. Chilton, B. Moubaraki, B. F. Abrahams, L. F. Chibotaru and K. S. Murray, *Angew. Chem., Int. Ed.*, 2013, **52**, 12014–12019.
115 S. K. Langley, D. P. Wielechowski, V. Vieru, N. F. Chilton, B. Moubaraki, L. F. Chibotaru and K. S. Murray, *Chem. Sci.*, 2014, **5**, 3246–3256.

116 S. K. Langley, D. P. Wielechowski, V. Vieru, N. F. Chilton, B. Moubaraki, L. F. Chibotaru and K. S. Murray, *Chem. Commun.*, 2015, **51**, 2044–2047.
117 S. K. Langley, D. P. Wielechowski, N. F. Chilton, B. Moubaraki and K. S. Murray, *Inorg. Chem.*, 2015, **54**, 10497–10503.
118 S. K. Langley, N. F. Chilton, B. Moubaraki and K. S. Murray, *Inorg. Chem.*, 2013, **52**, 7183–7192.
119 A. Swain, R. Martin, K. R. Vignesh, G. Rajaraman, K. S. Murray and S. K. Langley, *Dalton Trans.*, 2021, **50**, 12265–12274.
120 J. Long, F. Habib, P.-H. Lin, I. Korobkov, G. Enright, L. Ungur, W. Wernsdorfer, L. F. Chibotaru and M. Murugesu, *J. Am. Chem. Soc.*, 2011, **133**, 5319–5328.
121 N. Ishikawa, M. Sugita and W. Wernsdorfer, *J. Am. Chem. Soc.*, 2005, **127**, 3650–3651.
122 Y. C. Chen, J. L. Liu, W. Wernsdorfer, D. Liu, L. F. Chibotaru, X. M. Chen and M. L. Tong, *Angew. Chem., Int. Ed.*, 2017, **56**, 4996–5000.
123 S. Demir, I.-R. Jeon, J. R. Long and T. D. Harris, *Coord. Chem. Rev.*, 2015, **289**, 149–176.
124 N. Ishikawa, M. Sugita, T. Okubo, N. Tanaka, T. Iino and Y. Kaizu, *Inorg. Chem.*, 2003, **42**, 2440–2446.
125 N. Ishikawa, M. Sugita, N. Tanaka, T. Ishikawa, S.-Y. Koshihara and Y. Kaizu, *Inorg. Chem.*, 2004, **43**, 5498–5500.
126 N. Ishikawa, M. Sugita and W. Wernsdorfer, *Angew. Chem., Int. Ed.*, 2005, **44**, 2931–2935.
127 A. L. Wysocki and K. Park, *Inorg. Chem.*, 2020, **59**, 2771–2780.
128 R. Barhoumi, A. Amokrane, S. Klyatskaya, M. Boero, M. Ruben and J.-P. Bucher, *Nanoscale*, 2019, **11**, 21167–21179.
129 T. Morita, M. Damjanović, K. Katoh, Y. Kitagawa, N. Yasuda, Y. Lan, W. Wernsdorfer, B. K. Breedlove, M. Enders and M. Yamashita, *J. Am. Chem. Soc.*, 2018, 140, 2995–3007.
130 J. D. Rinehart, M. Fang, W. J. Evans and J. R. Long, *J. Am. Chem. Soc.*, 2011, **133**, 14236–14239.
131 T. Rajeshkumar and G. Rajaraman, *Chem. Commun.*, 2012, **48**, 7856–7858.
132 T. Gupta, T. Rajeshkumar and G. Rajaraman, *Phys. Chem. Chem. Phys.*, 2014, **16**, 14568–14577.
133 M. K. Singh, N. Yadav and G. Rajaraman, *Chem. Commun.*, 2015, **51**, 17732–17735.
134 Z. Hu, B.-W. Dong, Z. Liu, J.-J. Liu, J. Su, C. Yu, J. Xiong, D.-E. Shi, Y. Wang and B.-W. Wang, *J. Am. Chem. Soc.*, 2018, **140**, 1123–1130.
135 G. Velkos, D. Krylov, K. Kirkpatrick, X. Liu, L. Spree, A. Wolter, B. Büchner, H. Dorn and A. Popov, *Chem. Commun.*, 2018, **54**, 2902–2905.
136 Y. Wang, J. Xiong, J. Su, Z. Hu, F. Ma, R. Sun, X. Tan, H.-L. Sun, B.-W. Wang and Z. Shi, *Nanoscale*, 2020, **12**, 11130–11135.
137 G. Velkos, D. S. Krylov, K. Kirkpatrick, L. Spree, V. Dubrovin, B. Büchner, S. M. Avdoshenko, V. Bezmelnitsyn, S. Davis and P. Faust, *Angew. Chem., Int. Ed.*, 2019, **58**, 5891–5896.
138 F. Liu, L. Spree, D. S. Krylov, G. Velkos, S. M. Avdoshenko and A. A. Popov, *Acc. Chem. Res.*, 2019, **52**, 2981–2993.
139 F. Liu, D. S. Krylov, L. Spree, S. M. Avdoshenko, N. A. Samoylova, M. Rosenkranz, A. Kostanyan, T. Greber, A. U. Wolter and B. Büchner, *Nat. Commun.*, 2017, **8**, 16098.
140 F. Liu, G. Velkos, D. S. Krylov, L. Spree, M. Zalibera, R. Ray, N. A. Samoylova, C.-H. Chen, M. Rosenkranz and S. Schiemenz, *Nat. Commun.*, 2019, **10**, 571.
141 S. Dey and G. Rajaraman, *Chem. Sci.*, 2021, **12**, 14207–14216.
142 L. E. Darago, M. D. Boshart, B. D. Nguyen, E. Perlt, J. W. Ziller, W. W. Lukens, F. Furche, W. J. Evans and J. R. Long, *J. Am. Chem. Soc.*, 2021, **143**, 8465–8475.
143 C. Das, A. Upadhyay and M. Shanmugam, *Inorg. Chem.*, 2018, **57**, 9002–9011.
144 C. P. Burns, X. Yang, J. D. Wofford, N. S. Bhuvanesh, M. B. Hall and M. Nippe, *Angew. Chem., Int. Ed.*, 2018, **130**, 8276–8280.
145 A. Swain, A. Sen and G. Rajaraman, *Dalton Trans.*, 2021, **50**, 16099–16109.
146 M. Magott, M. Brzozowska, S. Baran, V. Vieru and D. Pinkowicz, *Nat. Commun.*, 2022, **13**, 2014.
147 C. A. Gould, K. R. McClain, D. Reta, J. G. Kragskow, D. A. Marchiori, E. Lachman, E.-S. Choi, J. G. Analytis, R. D. Britt and N. F. Chilton, *Science*, 2022, **375**, 198–202.
148 A. S. Zyazin, J. W. van den Berg, E. A. Osorio, H. S. van der Zant, N. P. Konstantinidis, M. Leijnse, M. R. Wegewijs, F. May, W. Hofstetter and C. Danieli, *Nano Lett.*, 2010, **10**, 3307–3311.
149 J. Hu and R. Wu, *Phys. Rev. Lett.*, 2013, **110**, 097202.
150 A. Sarkar and G. Rajaraman, *Chem. Sci.*, 2020, **11**, 10324–10330.
151 F. S. Guo, B. M. Day, Y. C. Chen, M. L. Tong, A. Mansikkamäki and R. A. Layfield, *Angew. Chem., Int. Ed.*, 2017, **129**, 11603–11607.
152 A. J. Brown, D. Pinkowicz, M. R. Saber and K. R. Dunbar, *Angew. Chem., Int. Ed.*, 2015, **127**, 5962–5966.
153 S. Sasmal, S. Hazra, P. Kundu, S. Dutta, G. Rajaraman, E. C. Sañudo and S. Mohanta, *Inorg. Chem.*, 2011, **50**, 7257–7267.
154 M. Trif, F. Troiani, D. Stepanenko and D. Loss, *Phys. Rev. Lett.*, 2008, **101**, 217201.
155 M. F. Islam, J. F. Nossa, C. M. Canali and M. Pederson, *Phys. Rev. B: Condens. Matter Mater. Phys.*, 2010, **82**, 155446.
156 C. A. Vaz, *J. Condens. Matter Phys.*, 2012, **24**, 333201.
157 I. Mihai Miron, G. Gaudin, S. Auffret, B. Rodmacq, A. Schuhl, S. Pizzini, J. Vogel and P. Gambardella, *Nat. Mater.*, 2010, **9**, 230–234.
158 R. Bircher, G. Chaboussant, C. Dobe, H. U. Güdel, S. T. Ochsenbein, A. Sieber and O. Waldmann, *Adv. Funct. Mater.*, 2006, **16**, 209–220.
159 M. S. Norre, C. Gao, S. Dey, S. K. Gupta, A. Borah, R. Murugavel, G. Rajaraman and J. Overgaard, *Inorg. Chem.*, 2019, **59**, 717–729.
160 T. Song, Z. Fei, M. Yankowitz, Z. Lin, Q. Jiang, K. Hwangbo, Q. Zhang, B. Sun, T. Taniguchi and K. Watanabe, *Nat. Mater.*, 2019, **18**, 1298–1302.
161 G. Cucinotta, M. Perfetti, J. Luzon, M. Etienne, P. E. Car, A. Caneschi, G. Calvez, K. Bernot and R. Sessoli, *Angew. Chem., Int. Ed.*, 2012, **51**, 1606–1610.
162 M. Briganti, G. F. Garcia, J. Jung, R. Sessoli, B. Le Guennic and F. Totti, *Chem. Sci.*, 2019, **10**, 7233–7245.
163 M. Briganti and F. Totti, *Dalton Trans.*, 2021, **50**, 10621–10628.
164 C. Ederer and N. A. Spaldin, *Phys. Rev. B: Condens. Matter Mater. Phys.*, 2007, **76**, 214404.
165 H.-L. Zhang, Y.-Q. Zhai, L. Qin, L. Ungur, H. Nojiri and Y.-Z. Zheng, *Matter*, 2020, **2**, 1481–1493.
166 J. Lu, M. Guo and J. Tang, *Chem. – Asian J.*, 2017, **12**, 2772–2779.
167 L. Ungur, S.-Y. Lin, J. Tang and L. F. Chibotaru, *Chem. Soc. Rev.*, 2014, **43**, 6894–6905.
168 A. Soncini and L. F. Chibotaru, *Phys. Rev. B: Condens. Matter Mater. Phys.*, 2008, **77**, 220406.
169 J. Tang, I. Hewitt, N. Madhu, G. Chastanet, W. Wernsdorfer, C. E. Anson, C. Benelli, R. Sessoli and A. K. Powell, *Angew. Chem., Int. Ed.*, 2006, **118**, 1761–1765.
170 L. F. Chibotaru, L. Ungur and A. Soncini, *Angew. Chem., Int. Ed.*, 2008, **120**, 4194–4197.
171 P.-H. Guo, J.-L. Liu, Z.-M. Zhang, L. Ungur, L. F. Chibotaru, J.-D. Leng, F.-S. Guo and M.-L. Tong, *Inorg. Chem.*, 2012, **51**, 1233–1235.
172 L. Ungur, S. K. Langley, T. N. Hooper, B. Moubaraki, E. K. Brechin, K. S. Murray and L. F. Chibotaru, *J. Am. Chem. Soc.*, 2012, **134**, 18554–18557.
173 G. Novitchi, G. Pilet, L. Ungur, V. V. Moshchalkov, W. Wernsdorfer, L. F. Chibotaru, D. Luneau and A. K. Powell, *Chem. Sci.*, 2012, **3**, 1169–1176.
174 J. Wu, X.-L. Li, M. Guo, L. Zhao, Y.-Q. Zhang and J. Tang, *Chem. Commun.*, 2018, **54**, 1065–1068.
175 G. Fernandez Garcia, D. Guettas, V. Montigaud, P. Larini, R. Sessoli, F. Totti, O. Cador, G. Pilet and B. Le Guennic, *Angew. Chem., Int. Ed.*, 2018, **130**, 17335–17339.
176 Q. Yang, L. Ungur, W. Wernsdorfer and J. Tang, *Inorg. Chem. Front.*, 2022, **9**, 784–791.
177 S. K. Langley, K. R. Vignesh, B. Moubaraki, G. Rajaraman and K. S. Murray, *Chem. – Eur. J.*, 2019, **25**, 4156–4165.
178 K. R. Vignesh and G. Rajaraman, *ACS Omega*, 2021, **6**, 32349–32364.
179 K. R. Vignesh, A. Soncini, S. K. Langley, W. Wernsdorfer, K. S. Murray and G. Rajaraman, *Nat. Commun.*, 2017, **8**, 1023.
180 K. R. Vignesh, S. K. Langley, A. Swain, B. Moubaraki, M. Damjanović, W. Wernsdorfer, G. Rajaraman and K. S. Murray, *Angew. Chem., Int. Ed.*, 2018, **130**, 787–792.
181 J. M. Ashtree, I. Borilović, K. R. Vignesh, A. Swain, S. H. Hamilton, Y. L. Whyatt, S. L. Benjamin, W. Phonsri, C. M. Forsyth and W. Wernsdorfer, *Eur. J. Inorg. Chem.*, 2021, 435–444.

